acta physica slovaca vol. 69 No. 2, 75 – 146 **2019**

LOCALIZED MAGNETIC MODELS WITH HIGHER-ORDER INTERACTIONS

Viliam Štubňa[a,b,1], **Michal Jaščur**[a,2]
[a] *Department of Theoretical Physics and Astrophysics, Faculty of Science, P. J. Šafárik University in Košice, Park Angelinum 9, 040 01 Košiice, Slovakia*
[b] *Gymnázium, Javorová 16, 052 01 Spišská Nová Ves, Slovakia*

Received 7 November 2019, accepted 12 November 2019

Investigation of the higher-order exchange interactions in magnetic spin systems has received during last decades increasing attention. In fact, many experimental studies have recently reported physical phenomena that cannot be explained using the standard approach based on theoretical models with pair interactions only. For this reason a lot of effort has been directed to the development theoretical models that may account for higher-order interaction energy terms. In this work we extensively review recent development in this interesting research field with the special emphasis on the works dealing with magnetic systems with higher-order spin interactions. A special attention is payed to the classification of the four-spin interactions that play an important role in magnetic spin systems. The substantial part of this contribution deals with the review of recent theoretical results obtained for various exactly solvable mixed-spin Ising models on decorated lattices. The particular attention is directed to understanding the influence of a special kind of higher-order interaction which is usually called as a three-site four-spin interaction. This interaction among other interesting physical effects also reveals a possible link between higher-order spin interactions and magneto-elastic properties of various real magnetic compound.

KEYWORDS: Mixed-spin Ising model, Exact results, Mapping transformations, Critical behavior, Higher-order spin interaction, Three-site four-spin interaction, Magneto-elastic properties

Contents

[1]E-mail address: viliamstubna@yahoo.com
[2]E-mail address: michal.jascur@upjs.sk

1 Introduction

The solid state physics deals with systems consisting of huge number of atoms that usually are not independent, instead they interact in a complex manner. In fact, the explanation of various interesting phenomena observed in diverse physical systems frequently requires the introduction of many-body interactions that represent a natural generalization of standard pair interactions (see for example [1], [2], [3], [4]). The relevant interaction energy of such many-body systems must then naturally include physical quantities of each individual atom. Consequently, the mathematical form of interaction energy is too much complex and for this reason it is very frequently approximated by the expression consisting of two-body terms only. Nevertheless, neglecting of the higher-order interactions terms has been in many cases found as a very crude approach providing inadequate description of underlying physical phenomena. This finding has initiated the growing interest in development theories going beyond the standard pair approximation. In general, accounting for the higher-order interaction terms is very hard problem of theoretical physics and requires development of new analytical and computational methods.

On the other hand, the localized magnetic models (for example Ising or Heisenberg) represent rare exceptions in this field of study, since the inclusion of higher-order interaction terms can be performed in a simple and straightforward manner and in some cases, even exact theoretical treatment of these models is possible [5–8]. Moreover, the experimental devices and methods have been recently substantially improved towards detecting physical effects caused by higher-order interactions in magnetic systems.

Although the original assumption of the higher-order interactions in magnetic processes come already in 1960-70 [9–11], their understanding is nowadays far from being settled in a clear way. There are many reasons to investigate implications and also the origin of the higher-order spin coupling. In connection with that, the study of physical properties of the higher-order exchange interaction may be essential for thorough understanding of its role in the magnetic systems.

In the present work we at first give a more detailed overview of magnetic systems with higher-order spin interaction and then in Sec. 3 we make classification of the four-order spin interactions that are the most important multispin interactions for explanation experimental data of various experimental compounds [12–21]. Among many other issues, we pay a special attention to the explanation of so-called three-site four-spin interaction, that will be studied in detail in the second part of this work. In order to investigate theoretically the novel physics related to three-site four-spin interactions, we at first review the method of algebraic transformations and then in Sec. 5-8 we discuss exact results obtained by this method for several mixed-spin Ising decorated models. Finally, in the last part we present the most important conclusions and comments on future perspectives of this research field.

2 Magnetic spin systems with higher-order interactions

Among the research works dealing with many-body interactions, those ones devoted to the investigation of multi-spin interactions in localized magnetic spin systems will be of our particular interest in this paper.

Intuitively it is clear that the first nontrivial contribution to the energy of of the localized magnetic system should come from the four-spin interactions. An exemplary case of such a system is the solid ^3He in which the relevant magnetic ordering is explained with the help of four-spin interactions [22]. The theoretical models with four-spin interactions were also successfully applied to such magnetic systems as NiS_2 and C_6Eu [23].

On the other hand, from the theoretical point of view, the essential papers in the field of higher-order spin interactions were published by Iwashita and Uryu, who discussed a number of such spin models and developed the corresponding theory [24–26]. In addition to the above mentioned contributions, many theoretical works analyzed Ising models with competing bilinear and multi-spin interactions using the different methods, such as exact calculations, [5–8], series expansion techniques [27–33], Frank-Mitran theory [34–36], renormalization group analysis [37], effective-field theory [38], mean-field theory [39] and Monte Carlo simulations [40, 41]. Finally, let us mention extraordinary interesting series of papers published by Köbler et al. [12–21] clarifying, both theoretically and experimentally, the impact of higher-order spin interaction in magnetic systems.

The common feature of all above mentioned theories is the use of various versions of Heisenberg or Ising spin models. Although, these models have been introduced many decades ago, their complex variants are the subject of very active research even nowadays. The pleasant mathematical feature of both models is their ability to incorporate higher-order and multi-spin interactions beyond the standard pair interaction terms. However, while some one-dimensional versions of the Heisenberg model are exactly solvable, in higher dimensions even applications of approximate methods are pretty much difficult. On the other hand, the solutions of Ising models are usually easily attainable using standard methods of statistical mechanics. The simplicity of the Ising model naturally leads to its extraordinary wide applicability in diverse fields of research. For example, in the condensed matter theory, the Ising model was applied for the description of many real materials, such as:

- lithium terbium tetrafluoride $LiTbF_4$,
- dysprosium monoaluminate $DyAlO_3$,
- dysprosium aluminium garnet $Dy_3Al_5O_{12}$,
- dysprosium ethyl sulfate (DyES) $Dy(C_2H_5SO_4)_3.9H_2O$, etc..
- dysprosium phosphate $DyPO_4$,
- potassium cobalt fluoride K_2CoF_4,
- rubidium tetrafluorocobaltate Rb_2CoF_4,

Several of these materials are very promising refrigerants and at present they are widely investigated [42]. The real materials, behaving similarly to the Ising model use to be referred as Ising-like materials to. A lot of Ising-like materials are discussed in the review by Wolf [43], where one can find the experimental data for thermal dependencies of magnetic susceptibility, specific heat and entropy.

The additional value of the Ising model is related to the fact that various one-dimensional and two-dimensional variants of the model are exactly solvable. The exact analytical results of these models then enable to study phase transitions and critical phenomena in detail, including some

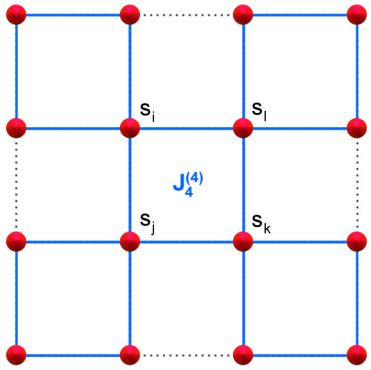

Fig. 2.1: Outline of the plaquette-type four-spin interaction on the square lattice (also called a four-site ring-exchange), which may be composed of two interpenetrating sublattices.

modern topics like frustrations or universality hypothesis [44–51]. Another class of Ising model systems, namely the diluted magnetic systems, are also very close to the real physical materials [3]. These materials involve the structural impurities into system which, under certain conditions, are able to change the behavior of a system significantly.

As already mentioned above, one of the most useful features of the Ising model is its ability to incorporate additional energy terms without any significant raising of the calculation complexity. For this reason, various Ising models represent the most studied models in statistical mechanics.

It order to illustrate the incorporation of multi-spin interactions into Ising model, one can express the total Hamiltonian of such a complex system in the form

$$\mathcal{H} = -J_2 \sum_{\langle i,j \rangle} s_i s_j - J_4 \sum_{\langle i,j,k,\ell \rangle} s_i s_j s_k s_\ell, \tag{2.1}$$

where in the simplest possible case, the spin variables s_i take the values of ± 1, $\forall i$. Clearly, the first summation in previous equation represents the energy contribution from traditional pair interactions and the second term describes plaquette-like four-spin four-site exchange interactions, just as it is shown in Fig. 2.1. Here, one should emphasize that the majority of theoretical studies in the condensed matter is initiated by experimental data obtained for various magnetic systems. Therefore, we will now continue further with the discussion of relevant experimental works devoted to the investigation of magnetic systems with higher-order interactions.

The absolute values of higher-order exchange interactions are usually markedly smaller comparing to the conventional two-spin ones. Based on experiments and also theoretical treatments, which we will mention in the following sections, the ratio of fourth-order to two-order interaction J_4/J_2 is assumed to be only $\sim 1-5\%$ in the most cases and $\sim 10-50\%$ in rare cases. One

[3] For example I. Syozi [52] has treated exactly an Ising model for an annealed system and obtained the numerical data for the critical concentration and the specific heat, which are fairly coincident with the experimental results for $Mn(HCOO)_2 \cdot 2H_2O$ diluted by nonmagnetic magnesium salt obtained by Matsuura et al. [53, 54].

might, of course, wonder how such a weak interaction can be detected by the magnetization measurements. And indeed, the obvious magnetization experiments are usually not able to confirm such weak effects, however, in many cases experimental results of magnetic systems [4], significantly differ from predictions of the conventional theoretical models, such as Heisenberg and Ising models with pair interactions. The representative example of such systems is Gd_2CuO_4 exhibiting the complex magnetic phase diagram consisting of at least four distinct magnetic phases, the weak ferromagnetism, etc. [55].

Furthermore, several physical conditions have been found, at which the higher-order exchange interactions take an important role and may also be experimentally detected. These are primarily: the large spin value (i.e., enough electrons per atom involved into interactions), fairly large orbital overlaps and the appropriate arrangement of a system, which should be able easily modified by introducing weak interactions in order to see fine changes in the experiments. For example, the system of spins on the antiferromagnetic triangular lattice which forms a so-called frustrated spin lattice, represents such a case [56].

One of the most clear evidence of the four-spin interaction was reported for the solid ^3He by detailed measurements of the low-field antiferromagnetic resonance spectrum of the spin-ordered phase [57]. The anomalous magnetic properties and structure was explained well by Roger et al. [58] by considering the strong four-spin exchange interaction caused by the large quantum fluctuations of the ^3He atoms. They showed, that two parameter model with the three-spin exchange and the planar four-spin exchange agrees quantitatively well with the experimental results, when assuming their magnitudes in levels $J_3 \sim -0.1, \quad J_4 \sim -0.355$. It should be also noticed, that the spin structures on liquid ^4He surface are also expected to be originated by the four-order interaction [59].

The nickel persulphide NiS_2 is a semiconductor with the anomalous magnetic behavior, in which Ni^{2+} ions form the fcc lattice with antiferromagnetic type of interaction. The neutron powder diffraction data collected by Hastings and Corliss [60] on NiS_2 show the transition at 40K to the structure which can be described as the antiferromagnetic ordering of the first kind. This is followed by the abrupt transition at 30K where additional diffraction peaks appear and these are consistent with the antiferromagnetic ordering of the second kind. Also in another neutron diffraction measurements [61] by Miyadai et al., which were performed on two single crystals of NiS_2 at low temperatures, such two types of the antiferromagnetic reflections was observed. Simultaneously, the weak ferromagnetism was revealed along with a small tetragonal deformation observed by Nagata et al. at the low temperature phase [62]. The appropriate spin Hamiltonian with the four-spin interaction qualitatively explaining aforementioned behavior of NiS_2 was established by Yosida and Inagaki [63].

The large elastic effects was observed [64] in ferromagnetic $GdAl_2$ or GdZn at the temperatures $T < T_c$ and it was proposed that these magnetoelastic properties for Gd^{3+} ions are due to the combination of the higher-order exchange interactions, the exchange striction and the domain-wall stress effect.

Next interesting compounds are CeSb [65] and $PrCo_2Si_2$ [66] in which the ordinary spin models do not explain the existence of zero magnetization layers or partially disordered phase, respectively. However, it was shown by Muraoka that it may be possible to explain these experimental results by introducing higher-order spin interactions [67].

[4] weak ferromagnetism, distortion of the ideal crystal structure, magnetic plateos, etc.

For some types of multilayer structures ($\mathtt{Al}-, \mathtt{Au}-$interlayers) it turns out, that the observed biquadratic coupling is intrinsic to the ideal multilayer structure rather than due to impurities or structural defects. Slonczewski model [68], assuming the non-Heisenberg exchange coupling including a biquadratic term, permits an interpretation of bi-quadratic coupling data [69] obtained by Gutierrez et al. for $\mathtt{Fe/Al/Fe} - \mathtt{trilayers}$ and of Fußet al. for $\mathtt{Fe/Au/Fe}$.

Similarly, the high degeneracy of spin states of the symmetrical $[\mathtt{Fe_3(II)Fe(III)}]$ cluster[5] was examined by Belinsky [70]. The classification of the spin states revealed the origin of degeneracy and the necessity to take into account the non-Heisenberg exchange interaction, namely a biquadratic one.

A sequence of unconventional phase transitions, namely the higher-temperature transition to an incommensurate state, was observed by Lin et al. [71] in $\mathtt{UNi_2Si_2}$. Subsequently, Mailhot et al. [72] showed the importance of biquadratic exchange, which is able to stabilize the sequence of phases period and leads also to the transition found in [71]. The thermal expansion and magnetostriction measurements was also done and reported by Zochowski [73] for the single-crystal $\mathtt{UNi_2Si_2}$.

Finally, let us mention several experimental works, where the higher-spin interaction was discussed in detail:

1. High field magnetization measurements [56] of the europium-graphite intercalation compound $\mathtt{C_6Eu}$ showed the existence of weak four-spin exchange interaction in addition to the usual bilinear one. Let us remark, that $\mathtt{Eu}$ atoms have the spin $S = 7/2$.

2. Shiroka et al. [74] found that the magnetic behavior in $\mathtt{C_6Eu}$ is largely driven by the in-plane antiferromagnetic and out-of-plane ferromagnetic interactions among the $\mathtt{Eu}^{2+}$ ions in co-operation with higher-order exchange interactions. Recent zero-field μSR measurements (muon spectroscopy) confirmed this picture [75].

3. Köbler et al. [21] presented experimental results on magnetic behavior of several three-dimensional magnetic materials. It was observed that discontinuous phase transitions and the magnon gap of the magnets with integer spin can be considered as signatures of the higher-order interactions such as the four-spin interactions. Concluding from these experiments, the higher-order interactions seem to be especially important in three-.dimensional systems.

[5] the iron core of the $[\mathtt{Fe_4S_4}]^+$ center

3 Classification of fourth-order exchange interactions

The most important class of the higher-order interactions from the experimental point of view is that one of the fourth-order exchange interactions. This class of the exchange interactions includes biquadratic, four-site four-spin and three-site four-spin interactions. The schemes of these interactions are depicted in Fig. 3.1. With respect to the number of sites and the number of spins involved in the interaction, the models with such interactions are sometimes called as $(2-2)$ model, $(2-4)$ model, $(4-4)$ model and $(3-4)$ one. Their local Hamiltonians along with the bilinear (two-order) one are listed in Tab. 3.1. The theoretical investigation of the multi-spin interactions is usually performed by means of approximate methods. Nevertheless, there are some exceptional contributions presenting exact solutions. Here one should mention

Exchange interaction	**Bond Hamiltonian**	Number of	
		sites	spins
bilinear (single)	$\mathcal{H}_i = -J_2^{(2)} \mathbf{S}_{i_1} \cdot \mathbf{S}_{i_2}$	(2)	2
biquadratic	$\mathcal{H}_i = -J_4^{(2)} \left(\mathbf{S}_{i_1} \cdot \mathbf{S}_{i_2}\right)^2$	(2)	4
four-site four-spin	$\mathcal{H}_i = -J_4^{(4)} \left(\mathbf{S}_{i_1} \cdot \mathbf{S}_{i_2}\right) \left(\mathbf{S}_{i_3} \cdot \mathbf{S}_{i_4}\right)$	(4)	4
three-site four-spin	$\mathcal{H}_i = -J_4^{(3)} \left(\mathbf{S}_{i_1} \cdot \mathbf{S}_{i_2}\right) \left(\mathbf{S}_{i_2} \cdot \mathbf{S}_{i_3}\right)$	(3)	4

Tab. 3.1: Fourth-order interactions Hamiltonians. The upper index of the interaction parameter J counts the number of sites, while the lowerone denotes the total number of spins involved in the interaction.

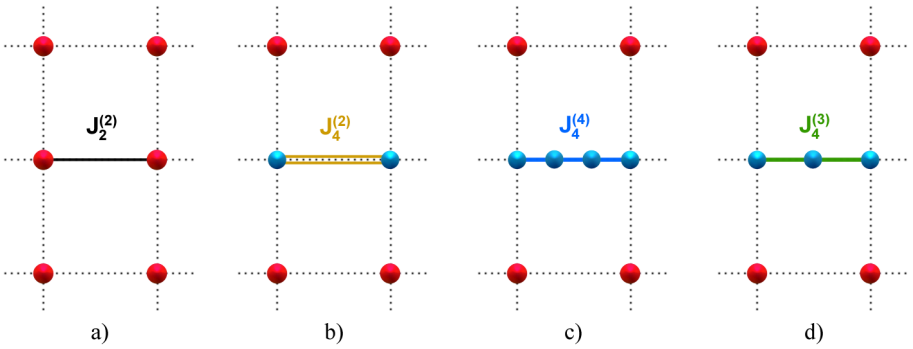

Fig. 3.1: The schemes of the fourth-order exchange interactions in comparison to bilinear interaction, as it is presented in [80]. Each full circle marks one atom and every line represents a kond of direct exchange interaction based on the overlap of electron wavefunctions. a) bilinear exchange interaction, b) biquadratic exchange interaction, c) four-site four-spin interaction, d) three-site four-spin interaction.

the papers published by Wu [76], Kadanoff and Wegner [77], Baxter [78]) and Baxter and Wu [79]. Probably the most surprising finding of these studies is the non-universal behavior of such models, since their critical exponents exhibit strong dependence on the parameters of relevant Hamiltonians.

Excepting the exact calculations, very much attention was also paid to the approximate methods due to their ability to describe the behavior of more complicated systems, which are closer to the real materials. In the following text, we will mention some interesting cases of such systems, which are based on the following generic types of Hamiltonians:

$$\mathcal{H} = -J_2^{(2)} \sum_{\langle ij \rangle} s_i s_j - J_4^{(2)} \sum_{\langle ij \rangle} \left(s_i s_j \right)^2 , \tag{3.1}$$

$$\mathcal{H} = -J_2^{(2)} \sum_{\langle ij \rangle} s_i s_j - J_4^{(3)} \sum_{\langle ijk \rangle} s_i s_j^2 s_k , \tag{3.2}$$

$$\mathcal{H} = -J_2^{(2)} \sum_{\langle ij \rangle} s_i s_j - J_4^{(4)} \sum_{\langle ijkl \rangle} s_i s_j s_k s_l , \tag{3.3}$$

where J_2 and J_4 represent the bilinear and four-spin exchange interactions, respectively, and s_α denotes the spin variable that can in general take $2S + 1$ values, corresponding to all possible spin projections along a given spatial axis.

3.1 Biquadratic interaction

The most frequently studied fourth-order exchange interaction is the biquadratic one. The biquadratic exchange is usually of very a small magnitude (≈ 0.05) comparing to the billinear exchange interaction, however, if it becomes significant, then even the one- dimensional spin systems may exhibit a rich phase diagram.

The correlation between the electrical conduction and ferromagnetism was empirically found in the certain compounds of manganese with the perovskite structure, e.g. manganese oxides such $\mathtt{La_{1-x}Sr_xMnO_3}$ or the mixed-valency structure $\left(\mathtt{La_xCa_{1-x}}\right)\left(\mathtt{Mn_x^{III}Mn_{1-x}^{IV}}\right)\mathtt{O_3}$ [81]. Zener interpreted it in terms of the principles governing the interaction of the d-shells of the transition metals [82]. Both, the electrical conduction and the ferromagnetic coupling in these compounds are found to arise from a double exchange process. This double exchange occurs indirectly by the spin interaction with mobile electrons traveling from one ion to other.

Harris and Owen described [10] the electron spin resonance spectrum of nearest-neighbor $\mathtt{Mn}^{2+}$ ion (spin $5/2$) pairs in $\mathtt{MgO}$. That resumed after previous resonance measurements, which indicated surprisingly large $\mathtt{Mn} - \mathtt{Mn}$ exchange interactions. Their analysis suggests, that in addition to the usual bilinear term in the form (3.1) there is also a bi-quadratic contribution to the exchange interaction present. The value of $J_4^{(2)}/J_2^{(2)} \approx 0.05$ was estimated.

Two additional examples, where the behavior of material reflects the bi-quadratic exchange contribution was given by Rodbell et al. [11]. They analyzed the temperature dependence of the sub-lattice magnetization in $\mathtt{MnO}$ and $\mathtt{NiO}$ oxides using a molecular field approach with the bi-quadratic exchange included. The authors reported markedly better results than those obtained

within the classical molecular field with the bi-linear exchange only. The magnitude of $J_4/J_2 \approx 0.02$ was suggested and also relevant phase transitions were calculated and classified to be of the first order.

In 1979, Iwashita and Uryu [83] studied the effects of the anisotropic biquadratic exchange interaction on the Curie temperature of a ferromagnet with the use of a simple pair model approximation (Oguchi approximation) [84]. Later, the general bilinear and biquadratic Hamiltonian of the form (3.1) was solved by Kulish et al. [85] using the Bethe Ansatz method for $J_4^{(2)}/J_2^{(2)} = 1$.

Moreover, the bilinear and biquadratic Hamiltonian was also used to describe the valence-bond solid ground state in antiferromagnets in one (and more) dimension by Affleck et al. [86]. Such a typical one-dimensional spin-1 antiferromagnet is for example $\mathtt{CsNiCl_3}$, which was already experimentally studied and exhibits an energy gap [87].

Finally, one should note the work by Mila and Zhang [88], who studied the mechanism for unusual predominant biquadratic interaction. They propose a new microscopic mechanism leading to the significant biquadratic interaction in spin-1 systems, which is suggested to be found in $\mathtt{LiVGe_2O_6}$.

3.2 Four-site four-spin interaction

Recently, the four-site four-spin interaction has been studied in several papers by the use of various methods. The Monte Carlo technique has been applied by Mouritsen [41] to investigate the critical behavior and phase transitions of the Ising model on the fcc lattice with mixtures of two- and four-spin interactions. In the limit of pure four-spin interactions the model exhibits a first-order transition.

The exact analysis of the magnetic ground states for spin-$1/2$ Ising models with pure four-spin interactions on the cubic lattices with Hamiltonian (3.3) was presented also by Mouritsen [89]. The ordered states found here encompass the ferromagnetic, antiferromagnetic, and ferrimagnetic phases. Two possible four-site four-spin configurations are for illustration shown in Fig. 3.2.

Jensen et al. [90] introduced another four-site four-spin Ising model in 3-dimensions on the simple-cubic lattice and treated it within the generalized mean-field approximation including short-range correlations. The phase diagram with various ordered structures including so- called $\langle 3, 1\rangle$ phase were discussed in this work. Similar results were also obtained by Grynberg and Ceva [91] using the Muller-Hartmann and Zittartz approximation and perturbation calculations.

Two-dimensional Ising $2 + m$ model with $m = 2, 3, 4$-spin interactions in the horizontal direction and the two-spin Ising interaction in the vertical direction on the square lattice was analyzed by Debierre and Turban [92] using the generalized mean-field approximation including short-range correlations and the phenomenological renormalization group approach. The self-duality of this model was indicated and confirmed. From that, when the transition is unique, then the free energy is singular along the same critical line as for $m = 2$ (i,e,, two-spin Ising model) and hence the formula $\sinh(2J_2^{(2)})\sinh(2J_m^{(m)}) = 1$ holds. Moreover, though the nature of the transition may change with m (the number of spins involved in the multi-spin interaction $J_m^{(m)}$), the critical line itself is not directly depending on m. Another interesting feature of this $2 + m$-spin Ising model is the possibility of exact prefacing transformation introduced by Berker (1975) to the conventional model with 2^{m-1} states per site and nearest-neighbor interactions.

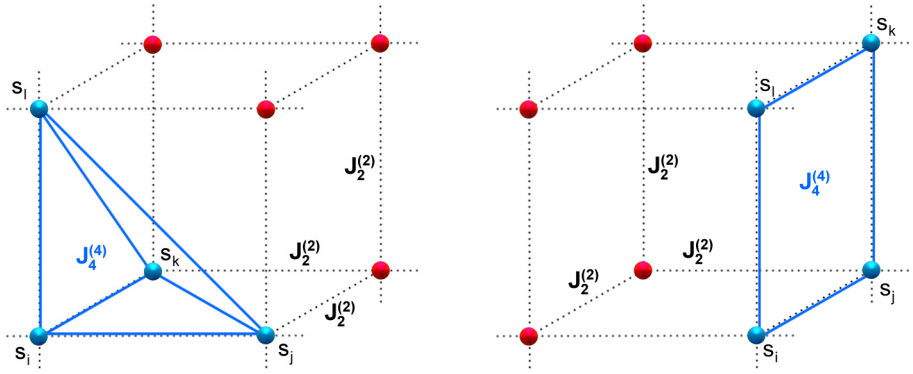

Fig. 3.2: Illustration of two different paths of four-spin exchange interaction $J_4^{(4)}$ for the cubic lattice, a) the "basic quartet" and b) the "plaquette wall". The four-spin interaction $J_4^{(4)}$ is indicated by blue line and bilinear $J_2^{(2)}$ interactions are drawn by black dotted lines between two sites.

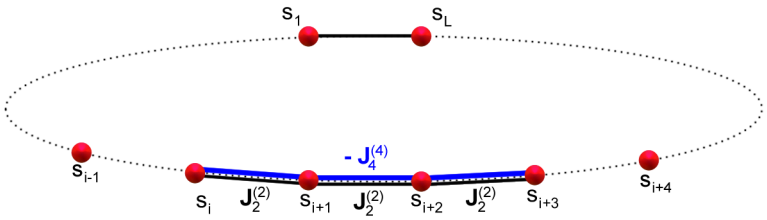

Fig. 3.3: Illustration of a periodically bounded finite-chain consisting of the L sites with the competing two and four-spin interactions.

[93]. Among these models, especially interesting and widely studied is the so called $2+4$ model. It involves the combination of competing two- and four-spin interactions, as depicted in Fig.3.3, and it has been the subject of several recent investigations in 1D version by Penson [94, 95]. A similar model in 2D has been studied by Grynberg, Ceva and Scott [96–98] (see Fig.3.4).

The alternative transfer-matrix representation was used by Grynberg and Ceva [96] to perform the phenomenological renormalization and finite-size scaling analysis of two-dimensional $2 + 4$ model with competing two and four-spin interactions in one direction. This approach enabled to obtain the leading eigenvalues of the transfer matrix with a significant saving of com-

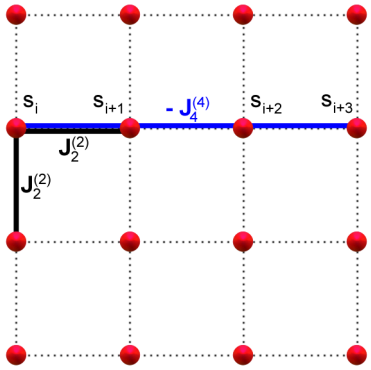

Fig. 3.4: Illustration of the interactions at $i-th$ site for two-dimensional $2+4$ model with competing two and four-spin interactions in $x-$direction.

puter time using the Lanczos scheme. The third eigenvalue of the transfer matrix gives the measure of interface free energy between the different phases that coexist along the transition line and provides the important information about order of phase transition.

The Ising model with higher-order interactions was also used for the theoretical description of bilayers with undulating surfaces. In lipid bilayers the low-temperature phases have turned out to be unusually rich in the structure in some cases, with sinusoidal undulations in the bilayer surface extending over several hundreds of angstroms. An interesting new approach to this problem was invented by Scott [98] by defining a two-dimensional lattice containing particles which have both, discrete and continuous degrees of freedom. Then, following the procedure previously applied to deformable lattice models, the variables are decoupled by the procedure which reduces the model to the simple Ising lattice with four-order spin interactions plus a harmonic oscillator. The Monte Carlo and mean-field data for such a four-spin model, depicted in Fig. 3.5, were also presented in the above mentioned paper.

In addition, the Monte Carlo simulations on the two-dimensional $2+4$ model with competing two and four-spin interactions was performed by Hernandez and Ceva [99], who studied the phase diagram, magnetization (both global and by column), susceptibility, energy, specific heat, correlation functions and some other quantities.

The phase diagram of the Ising square ferromagnet with nearest-neighbor, next-nearest-neighbor, and four-spin plaquette interactions were investigated using the cluster variation method in the square approximation by Buzano and Pretti [100]. and the two-dimensional Heisenberg model with four-spin and two-spin interactions on the square lattice was discussed by Sandvik using the ground-state projector quantum Monte Carlo simulations [101]. Next, using the extended Lee-Yang theorem and correlation inequalities, the four-spin interaction is discussed in [102] by Lebowitz and Ruelle in relation to the phase transition in an external field.

The mixed spin-1/2 and spin-1 Ising model with four-spin interactions as it is shown in Fig. 2.1 was investigated by Benayad and Ghliyem [103] within the finite cluster approxima-

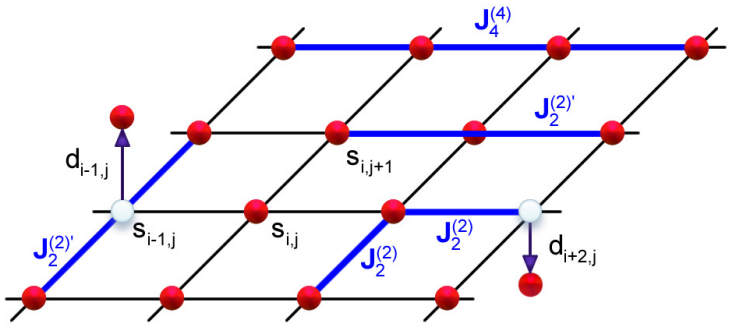

Fig. 3.5: Part of the two-dimensional lattice containing particles with both discrete and continuous degrees of freedom. Types of interactions that occur in a transformed Hamiltonian that has been used to the theoretical description of bilayers with undulating surfaces by Scott [98].

tion based on a single-site cluster theory on the square lattice. Several exact results were also worked out by Lacková and Jaščur, namely, mixed spin-1/2 and spin-S transverse Ising model with two- and four- spin interactions on the honeycomb lattice [104, 105] and the generalized Wu model with two- and four-spin interactions [106]. Most of these models are closely related to our recent investigations that will be presented in the following sections.

3.3 Three-site four-spin interaction

The three-site four-spin interaction, as a special case of the four-site four-spin interaction, takes the least attention despite of the fact that this interaction may lead to the most unconventional behavior, which in many cases has been observed also experimentally. Matveev and Nagaev [39] investigated the magnetic properties of a spin system with the three-site four-spin interaction by making use of the spin-wave theory and the mean-field approximation.

Later, Munro and Girardeau studied spin systems in the presence of single and double electron exchange with combined Hamiltonian (3.1) and (3.2) at nonzero temperature using the generalized mean field approximation for arbitrary spin [80]. The authors detected paramagnetic, ferromagnetic, anti- ferromagnetic and also partially ordered phases. Further, they concluded that as the the partially ordered phase becomes more prominent as the atomic spin increases.

Next, Iwashita and Uryu treated [107] the effects of the three-site four-spin interaction on square , simple cubic and body-centred cubic lattices with spins $s = 1$ and $s = 3/2$ applying the three-spin model approximation (the improved Oguchi approximation) with the Hamiltonian similar to (3.2). In 1991, the same authors investigated the three-site four-spin interaction on the triangular lattice with tha same Hamiltonian but with the second- neighbor interaction enhanced [24].

The ground state of a three-dimensional axial next-nearest neighbor Ising model with the three-site four-spin interaction were obtained rigorously by Muraoka et al. [67, 108] by means of

the transfer matrix method along with use of the Monte Carlo simulation with Fourier transformation for thermodynamic quantities.

The term x^2, observed experimentally in the susceptibility of diamagnetically diluted ferromagnetic composition series $\mathtt{Eu_xSr_{1-x}S}$, appears due to the ferromagnetic three-spin interactions, as it was discussed by Müller-Hartmann et al. [109]. A similar model was studied by Muraoka [110], where the finite-temperature magnetic-phase diagram of this compound was investigated by means of the site-dependent molecular-field approximation. The system exhibits the direct phase transition to the antiferromagnetic phase, which wasn experimentally observed in $\mathtt{UNi_2Si_2}$. This phase transition is accompanied by a drastic increase of the entropy in the antiferromagnetic state. The magnetic-field- temperature phase diagram is also in agreement with that one of $\mathtt{UNi_2Si_2}$. The pressure-temperature phase diagram for $\mathtt{UNi_2Si_2}$ was obtained by Honda [111] and Quirion et al. [112] and the results are very similar to the magnetic-field temperature phase diagram. Moreover, it seems that the effect of the pressure in $\mathtt{UNi_2Si_2}$ is the same as that one of the magnetic field.

Our previous discussion indicates that many experimental results of magnetic systems are poorly explainable by standard models with bilinear interactions, due to the lack of freely adjustable parameters. On the other hand, the models with higher-order exchange interactions are clearly capable to explain well the observed experimental results, including the description of various unconvetional phenomena in magnetic systems.

Nonetheless, due to its small magnitude, the measurements of higher-order exchange interactions are very difficult. In spite of that, there exist several materials in which such interactions were definitely confirmed. As the previous sections clearly illustrate, a number of experimental results in magnetic systems, still not well theoretically explained, pertains mainly the following phenomena:

- an unexpectedly high and slow varying magnetization
- unusually rich phase diagram
- a sequence of unconventional phase transitions
- magnetization plateaus
- partially ordered phases, etc..

Further, as recent papers have shown, the models with the higher-order exchange have provided in many cases markedly better results towards the real materials description than usual models with the bi-linear nearest and next-nearest neighbor interactions.

The aforementioned preliminary findings have been also inspirations for our research addressing higher-order interactions in spin systems, especially the three-site four-spin interaction.

3.4 Magnetostriction

The magnetostriction is a physical phenomenon observed in magnetic materials that causes the change of their shape depending on the magnetization. The magnetostrictiion coefficient $\lambda = \triangle l/l$ is defined as the fractional change in length as the magnetization increases from zero to

its saturation value. The magnetostriction can be positive or negative and its magnitude is of the order $|\lambda| \approx 10^{-5} - 10^{-6}$.

The effect of the magnetostriction was first identified in 1842 by James Joule by observing of an iron properties [113]. The effects of strain dependence on the isotropic exchange energy have been briefly mentioned by Néel [114], who has called it the exchange magnetostriction. It turns out, that the magnetistriction makes a more important contribution to the energy than it was previously recognized. For example, in MnAs or $\mathtt{Mn}_{1.96}\mathtt{Cr}_{0.04}\mathtt{Sb}$, the change of the length at the phase transition point is about 2% and 0.6%, respectively. The associated elastic energy is of the order of $10^1 - 10^2\, Jcm^{-3}$, which is comparable with the inter-atomic exchange energy. This is larger than the usual anisotropy energies, and under these conditions the exchange magnetostriction will dominate over the anisotropy energy.

The magnetostriction is one of the typical processes that are usually considered as a theoretical framework leading to the higher-order exchange interactions terms. Just by assuming the bilinear exchange interactions between the nearest-neighbor spins along with the magnetoelastic effect, the fourth-order exchange interactions arises naturally. Other such a framework is a perturbation expansion of the total Hamiltonian including free ions energy, the crystalline field energy, the spin-orbit coupling and the bilinear exchange interaction. However, especially in the case of magnetostriction, the genesis of the fourth-order exchange interactions is quite explanatory. For that reason, in the following short paragraphs we briefly outline several steps leading to the fourth-order exchange interactions terms for the simple systems of two and three particles.

a) System of two particles

Let us assume two magnetic atoms interacting via the exchange interaction J depending on the atomic separation r. Taking the approach, that has been used by Harris [115], the total energy E of the atomic pair with incorporated energy term of elastic displacement $r_0 \to r$ can be assumed in the form

$$E = J\left(r\right)\left(\mathbf{S}_{i_1} \cdot \mathbf{S}_{i_2}\right) + \frac{1}{2}\varepsilon\frac{\delta r^2}{r_0}, \tag{3.4}$$

where ε is an elastic constant and $\delta r = r - r_0$ means the separation between atoms. The equilibrium condition is then given by $\frac{dE}{dr} = 0$,, which means

$$\frac{dJ\left(r\right)}{dr}\left(\mathbf{S}_{i_1} \cdot \mathbf{S}_{i_2}\right) + \varepsilon\frac{\delta r}{r_0} = 0. \tag{3.5}$$

Now, one can only proceed further by making some assumption about dJ/dr. The simplest possibility is to assume that it remains constant over the whole range of the distortion, which is equivalent to taking just the first two terms of a Taylor's expansion of $J(r)$. In this way we obtain

$$E = J_0\left(\mathbf{S}_{i_1} \cdot \mathbf{S}_{i_2}\right) - \frac{1}{2}\frac{r_0}{\varepsilon}\left(\mathbf{S}_{i_1} \cdot \mathbf{S}_{i_2}\right)^2\left(\frac{dJ}{dr}\right)^2_{r=r_0}, \tag{3.6}$$

In the last formula for energy, the effective bi-quadratic term has arisen, however, due to the simplicity of calculation, the relevant results do not fit the experimental data accurately enough

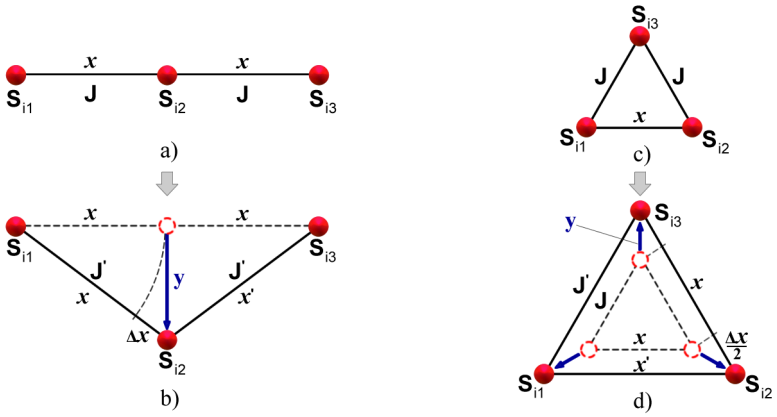

Fig. 3.6: The schemes of three particles spin system before and after shift. a), b) The shift of middle particle from linear arrangement behaving in magnetic compounds, c), d) The triangle cluster expansion by magnetoelastic effect present in complex compounds.

[115]. On the other hand, if one supposes $\frac{dJ(r)}{dr} = f(r)$, then the simple way of the dependence of J may be assumed as

$$J(r) = J_0 e^{-\kappa \frac{r}{r_0}}, \tag{3.7}$$

where κ is some positive constant. In this case, the theoretical results agree with the experimental ones with accuracy of the order $\pm 0.5\%$) [115].

Finally, we have to give a comment on the prefatory starting point of this procedure. By limiting treatment to only two atoms, we restrict the influence of striction δr to the one neighbor only, and for this reason, the appearance of higher-order interaction here is limited to the bi-quadratic term. This inaccuracy is better handled in the following approaches.

b) System of three particles - linear

Let us now consider a linear system of three particles as depicted in Fig. 3.6 a). Applying the approach that has been used by Iwashita [25, 26], one can make the following deduction.

Assuming just the spin-part of a wave function, the magnetic energy can be expressed in the form

$$E_m = J(\mathbf{S}_{i_1} \cdot \mathbf{S}_{i_2}) + J(\mathbf{S}_{i_2} \cdot \mathbf{S}_{i_3}), \tag{3.8}$$

where J is the bilinear exchange interaction and $\mathbf{S}_{i_1}, \mathbf{S}_{i_2}, \mathbf{S}_{i_3}$ denote to the spin-vector operators corresponding to the relevant particles.

Considering a temporary displacement of $2nd$ particle, just as illustrated in 3.6 b), the elastic potential energy is given by

$$E_p = \frac{1}{2} k y^2, \tag{3.9}$$

where $y = \sqrt{(x')^2 - x^2}$ is the displacement of $2nd$ particle with respect to the equilibrium position and k denotes the elastic constant. Consequently, the bilinear exchange interaction J will change ($J \to J'$) an by assuming small displacement, the new exchange interaction can be written in the form

$$J' = J\left[1 - \alpha \triangle x\right], \tag{3.10}$$

where $\triangle x = x' - x$ and α represents a dimensionless constant.

The total energy of the investigated system is then the sum of the elastic energy and the magnetic energy

$$\mathcal{E} = E_p + E_m, \tag{3.11}$$

and the free energy then may be generally written in the form

$$\mathcal{F} = \frac{1}{2}k\left[(x')^2 - x^2\right] + J\ \left[1 - \alpha\left(x' - x\right)\right]\left[\left(\mathbf{S}_{i_1} \cdot \mathbf{S}_{i_2}\right) + \left(\mathbf{S}_{i_2} \cdot \mathbf{S}_{i_3}\right)\right]. \tag{3.12}$$

The displacement of $2nd$ particle acquires its equilibrium value, when the free energy reaches its minimum with respect to x'. Thus, the equilibrium condition for the free energy is given by

$$\frac{\partial \mathcal{F}}{\partial x'} = 0 = kx' - J\alpha\left[\left(\mathbf{S}_{i_1} \cdot \mathbf{S}_{i_2}\right) + \left(\mathbf{S}_{i_2} \cdot \mathbf{S}_{i_3}\right)\right]. \tag{3.13}$$

Consequently, the equilibrium displacement of $2nd$ particle reads

$$x' = \frac{1}{k}\alpha J\left[\left(\mathbf{S}_{i_1} \cdot \mathbf{S}_{i_2}\right) + \left(\mathbf{S}_{i_2} \cdot \mathbf{S}_{i_3}\right)\right]. \tag{3.14}$$

Substituting (3.14) into the (3.12) we obtain

$$\begin{aligned} \mathcal{F} &= -\frac{1}{2}kx^2 + J_2\left[\left(\mathbf{S}_{i_1} \cdot \mathbf{S}_{i_2}\right) + \left(\mathbf{S}_{i_2} \cdot \mathbf{S}_{i_3}\right)\right] \\ &+ J_4\left[\left(\mathbf{S}_{i_1} \cdot \mathbf{S}_{i_2}\right)^2 + \left(\mathbf{S}_{i_2} \cdot \mathbf{S}_{i_3}\right)^2 + \left(\mathbf{S}_{i_1} \cdot \mathbf{S}_{i_2}\right)\left(\mathbf{S}_{i_2} \cdot \mathbf{S}_{i_3}\right) + \left(\mathbf{S}_{i_2} \cdot \mathbf{S}_{i_3}\right)\left(\mathbf{S}_{i_1} \cdot \mathbf{S}_{i_2}\right)\right], \end{aligned} \tag{3.15}$$

where the new interaction parameters, J_2 and J_4 take the form

$$J_2 = J\ (1 + \alpha x)\,,\ \ J_4 = -\frac{1}{2}\frac{\alpha^2 J^2}{k}. \tag{3.16}$$

c) System of three particles - triangle

The above mentioned procedure gives similar results also for complex compounds, which one can imagine as the interconnected version of system of three particles, as it is illustrated in Fig. 3.6 c). Hence, assuming the magnetostriction in the way of Fig. 3.6 d), one obtains the following

expression for the free energy

$$\begin{aligned}\mathcal{F} &= J_2\left[(\mathbf{S}_{i_1}\cdot\mathbf{S}_{i_2})+(\mathbf{S}_{i_2}\cdot\mathbf{S}_{i_3})+(\mathbf{S}_{i_3}\cdot\mathbf{S}_{i_1})\right] \\ &\quad +J_4\left[(\mathbf{S}_{i_1}\cdot\mathbf{S}_{i_2})^2+(\mathbf{S}_{i_2}\cdot\mathbf{S}_{i_3})^2+(\mathbf{S}_{i_3}\cdot\mathbf{S}_{i_1})^2\right] \\ &\quad +2J_4\left[(\mathbf{S}_{i_1}\cdot\mathbf{S}_{i_2})(\mathbf{S}_{i_2}\cdot\mathbf{S}_{i_3})+(\mathbf{S}_{i_2}\cdot\mathbf{S}_{i_3})(\mathbf{S}_{i_3}\cdot\mathbf{S}_{i_1})+(\mathbf{S}_{i_3}\cdot\mathbf{S}_{i_1})(\mathbf{S}_{i_1}\cdot\mathbf{S}_{i_2})\right],\end{aligned} \tag{3.17}$$

where the interaction parameters, J_2 and J_4 take again the form of (3.16).

Thus, as it can be seen in the equations (3.15) and (3.17), when one assumes additional degrees of freedom in a magnetic system, the bi-quadratic and three-site four-spin interactions may be natural components of energy expression.

4 Algebraic transformations

4.1 Decoration-iteration transformation

Methods of algebraic transformations represent a very useful tool for theoretical investigation various models in Statistical mechanics. Here we will mention two of them that have been recently widely applied to study magnetic properties of localized spin systems (see [116]).

At first let us briefly discuss the decoration-iteration transformation which has been originally introduced by Syozi [117] in 1951. This transformation is based on elimination of one atom (or a group of atoms) located between a couple of spins on each bond of crystalline lattice. After performing this transformation we obtain the lattice consisting only of spins located on sites of so called original lattice. The transformation works, of course, also in opposite direction, i.e., we can introduce one new atom (or a group of atoms) on each bond of a regular lattice and obtain a new complex lattice structure. The procedure of iterative introduction of new atoms is called as the lattice decoration, so that the procedure is known as the decoration-iteration transformation. The process of decorating one single bond of a lattice by one atom is illustrated in Fig. 4.1

Moreover, instead of bonds, we can in a similar manner decorate the sites of some regular lattice structure, however, in the following formulation we restrict ourselves to the bond-decorared systems. Although in any case such an transformation is apparently the local one, it can be used for calculations of all relevant thermodynamic quantities of the whole system. This important property follows from the fact that transformation can be exactly performed at the level of partition function of a decorated system, what enables to generate lots of new exactly solvable spin systems, including those with multispin and higher-order interactions.

The mathematical formulation of the transformation can be due to its locality performed in a very general manner as we will demonstrate in the following text for the case of one Ising-type decorating atom.

At first we express the total Hamiltonian of the decorated system as a sum of the the bond Hamiltonians, i.e.,

$$\mathcal{H}_d = \sum_{k=1}^{Nz/2} \mathcal{H}_k(S_k, \mu_{k1}, \mu_{k2}), \tag{4.1}$$

where N represents total number of atoms on the original (i.e., non-decorated lattice), z denotes its coordination number. and the summation runs over all bonds of non-decorated lattice. It is

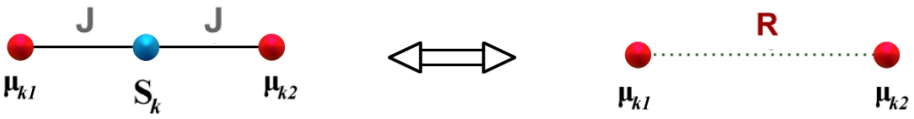

Fig. 4.1: The decoration-iteration transformation scheme.

clear that the bond Hamiltonian of the $\mathcal{H}_k$ must contain all energy contribution related to the k-th bond and in general it will explicitly depend on spin variables S_k of decorating atoms, two spin variables μ_{k1}, μ_{k2} of the original lattice (see Fig. 4.1) and it will of course contain also all relevant interaction parameters. Nonetheless, in order to keep the compact form of notation, we will omit the explicit dependence of site Hamiltonian on the exchange parameters.

Now, using Eq. (4.1) one can express the canonical partition function of the decorated system in the form

$$\mathcal{Z}_d = \sum_{\{\mu_{k\gamma}=\pm 1/2\}} \sum_{\{S_k\}} \exp(-\beta\mathcal{H}) = \sum_{\{\mu_{k\gamma}=\pm 1/2\}} \prod_{k=1}^{Nz/2} \sum_{S_k=-S}^{S} \exp\left[-\beta\mathcal{H}_k(S_k,\mu_{k1},\mu_{k2})\right], \tag{4.2}$$

where the curled brackets indicate the fact that relevant summation concerns all spin variables of the decorated lattice, S represents the spin of decorating atoms and $\beta = 1/(k_B T)$.

At this stage of calculation it is clear that summation over spin variable S_k on the r.h.s of (4.2) will always lead to the expression depending on the spin variables μ_{k1} and μ_{k2} and therefore one can apparently introduce the following relation

$$\sum_{S_k=-S}^{S} \exp\left[-\beta\mathcal{H}_k(S_k,\mu_{k1},\mu_{k2})\right] = A\exp(\beta R\mu_k\mu_{k2}). \tag{4.3}$$

Here A and R stand for unknown parameters that will be determined later. The previous equation represents, in fact, the decoration-iteration transformation and it enables to evaluate the partition function of decorated lattice if the corresponding partition function of non-decorated lattice is known. Indeed, substituting (4.3) back into r.h.s of Eq. (4.2) one obtains

$$\mathcal{Z}_d = A^{Nz/2} \sum_{\{\mu_{k\gamma}\}=\pm 1/2} \exp\left(\beta R \sum_k \mu_{k1}\mu_{k2}\right) = A^{Nz/2}\mathcal{Z}_0, \tag{4.4}$$

where $\mathcal{Z}_0$ represent the partition function of corresponding non-decorated lattice, which is described by the Hamiltonian $\mathcal{H}_0 = -R\sum_k \mu_{k1}\mu_{k2}$.

Let us now continue with the evaluation of parameters A and R. Since Eq. (4.3) must be satisfied for all possible values of μ_{k1} and μ_{k2}, then substituting $\mu_{k1} = \pm 1/2$ and $\mu_{k2} = \pm 1/2$ one obtains just two independent equations, namely,

$$\sum_{S_k=-S}^{S} \exp\left[-\beta\mathcal{H}_k(S_k,1/2,1/2)\right] = A\exp(\beta R/4). \tag{4.5}$$

and

$$\sum_{S_k=-S}^{S} \exp\left[-\beta\mathcal{H}_k(S_k,1/2,-1/2)\right] = A\exp(-\beta R/4). \tag{4.6}$$

From these relations one easily gets

$$A = \sqrt{w_1 w_2}, \quad \beta R = 2 \ln \left(\frac{w_1}{w_2} \right), \tag{4.7}$$

with

$$w_1 = \sum_{S_k=-S}^{S} \exp \left[-\beta \mathcal{H}_k(S_k, 1/2, 1/2) \right] \tag{4.8}$$

and

$$w_2 = \sum_{S_k=-S}^{S} \exp \left[-\beta \mathcal{H}_k(S_k, 1/2, -1/2) \right]. \tag{4.9}$$

As we can see, by selecting various bond Hamiltonians $\mathcal{H}_k$ one can generate almost unlimited number of new Ising-type models, the can be exactly solved if we are able to evaluate the partitions function of their corresponding non-decorated counterparts (see for example [116]). It also clear that Eqs. (4.5)-(4.9) are valid for arbitrary lattice structures, since they are derived from one common geometric structure (see Fig. 4.1).

Now, we can directly from the definition express the Helmholtz free energy in the form

$$F_d = -\frac{Nz}{2} k_B T \ln(A) + F_0, \tag{4.10}$$

where $F_0 = -k_B T \ln Z_0$ is the Helmholtz free energy of the original (non-decorated) lattice, which must be, of course, known in advance from some independent calculation. Further physical quantities of the decorated lattice, like entropy S_d, internal energy U_d and specific heat C_{Vd}, now follow directly from well-known thermodynamic relations, namely,

$$S_d = -\left(\frac{\partial F_d}{\partial T} \right)_V, \quad C_{Vd} = -T \left(\frac{\partial^2 F_d}{\partial T^2} \right)_V \quad \text{and} \quad U_d = F_d + T S_d. \tag{4.11}$$

All these thermodynamic quantities will be obviously different for different lattices, since they clearly depend on the topology of decorated (and also original) lattice. This fact will be demonstrated in following sections, where we will discuss our recent results for several specific models.

4.2 Star-triangle transformation

Before proceeding further, we briefly outline another algebraic transformation which is known as the star-triangle transformation and has been originally introduced by Onsager [118].

This transformation is graphically depicted in Fig. 4.2 and it is based on eliminating the central atom of a star, which interacts with three atoms located in its vertexes. After such an elimination, we obtain three atoms located at vertexes of a triangle and these atoms are mutually coupled by a new pair nearest-neighbor interaction. That is, why this procedure is called as the star-triangle or $Y - \Delta$ transformation.

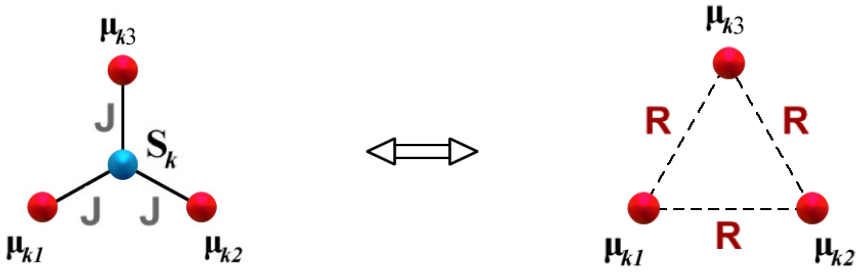

Fig. 4.2: The star-triangle transformation scheme.

In order to derive the mathematical formulas for $Y-\Delta$ transformation, we need just slightly modify our calculations done in previous subsection. The total Hamiltonian of the lattice consisting of star-like building units can be expressed as

$$\mathcal{H}_Y = \sum_{k=1}^{N} \mathcal{H}_k(S_k, \mu_{k1}, \mu_{k2}, \mu_{k3}), \tag{4.12}$$

where the dependence of local Hamiltonian $\mathcal{H}_k$ on exchange interactions has been for simplicity again omitted. The spin variable S_k can in general take $2S+1$ possible values (S being the spin of the central atom of the star) and all variables μ can take only values of $\pm 1/2$.

The partition function corresponding to the Hamiltonian $\mathcal{H}_Y$ can be written in the form

$$\begin{aligned} \mathcal{Z}_Y &= \sum_{\{\mu_{k\gamma}=\pm 1/2\}} \sum_{\{S_k\}} \exp(-\beta\mathcal{H}) \\ &= \sum_{\{\mu_{k\gamma}=\pm 1/2\}} \prod_{k=1}^{N} \sum_{S_k=-S}^{S} \exp\left[-\beta\mathcal{H}_k(S_k, \mu_{k1}, \mu_{k2}, \mu_{k3})\right]. \end{aligned} \tag{4.13}$$

Now introducing the standard $Y-\Delta$ transformation

$$\sum_{S_k=-S}^{S} \exp\left[-\beta\mathcal{H}_k(S_k, \mu_{k1}, \mu_{k2}, \mu_{k3})\right] = A\exp\left[\beta R(\mu_{k1}\mu_{k2}+\mu_{k1}\mu_{k3}+\mu_{k2}\mu_{k3})\right], \tag{4.14}$$

one easily rewrites Eq. (4.13) in the form

$$\mathcal{Z}_Y = A^N \sum_{\{\mu_{k\gamma}\}=\pm 1/2} \exp\left(\beta R \sum_k \mu_{k1}\mu_{k2}\right) = A^N \mathcal{Z}_\Delta, \tag{4.15}$$

where $\mathcal{Z}_\Delta$ denotes the partition function of the transformed lattice consisting of triangles and which is described by the Hamiltonian $\mathcal{H} = -R\sum_k \mu_{k1}\mu_{k2}$.

Repeating the same kind of calculations as those for the decorated lattice we simply get the following equations for unknown parameters A and R

$$A = \sqrt[4]{V_1 V_2^3}, \quad \beta R = \ln\left(\frac{V_1}{V_2}\right), \tag{4.16}$$

where we have defined two new functions

$$V_1 = \sum_{S_k=-S}^{S} \exp\left[-\beta \mathcal{H}_k(S_k, 1/2, 1/2, 1/2)\right] \tag{4.17}$$

and

$$V_2 = \sum_{S_k=-S}^{S} \exp\left[-\beta \mathcal{H}_k(S_k, 1/2, 1/2, -1/2)\right]. \tag{4.18}$$

The Helmholtz free energy takes now obviously the form

$$F_Y = -N k_B T \ln(A) + F_\Delta, \tag{4.19}$$

where $F_\Delta = -k_B T \ln \mathcal{Z}_\Delta$ and further thermodynamic quantities can be naturally calculated from the general relations (4.11).

5 Mixed spin Ising models with three-site four-spin interaction on the square lattice

5.1 Definition of the model

In order to demonstrate the role of the spin of decorating atoms, two particular models with $S = 1$ ans $S = 3/2$ will be now discussed in detail in accordance with the results obtained in [119–122]. Both models, that are defined on the decorated square lattice (see Fig. 5.1 a)), are obviously generic representatives of the decorated planar structures and for that reason they can be naturally solved exactly by decoration-iteration transformation. Moreover, the general formulation of the decoration-iterations transformation in Sec. 4 enables to derive relevant equations for both models in a unified manner.

In order to take into account the three-site four-spin interactions, one takes the bond Hamiltonian $\mathcal{H}_k$ in the form

$$\mathcal{H}_k = -J(\mu_{k1} + \mu_{k2})S_k - J'\mu_{k1}\mu_{k2} - J_4\mu_{k1}\mu_{k2}S_k^2 - DS_k^2, \tag{5.1}$$

where J denotes the nearest-neighbor and J' next- nearest-neighbor bilinear exchange interactions, J_4 represents the three- site four-spin exchange interaction and D stands for the single- ion anisotropy parameter. Substituting $z = 4$ and $\mathcal{H}_k$ into general formulation of Subsec. 4.1, one obtains for the partition function the following simple relation

$$\mathcal{Z} = A^{2N}\mathcal{Z}_0(\beta R). \tag{5.2}$$

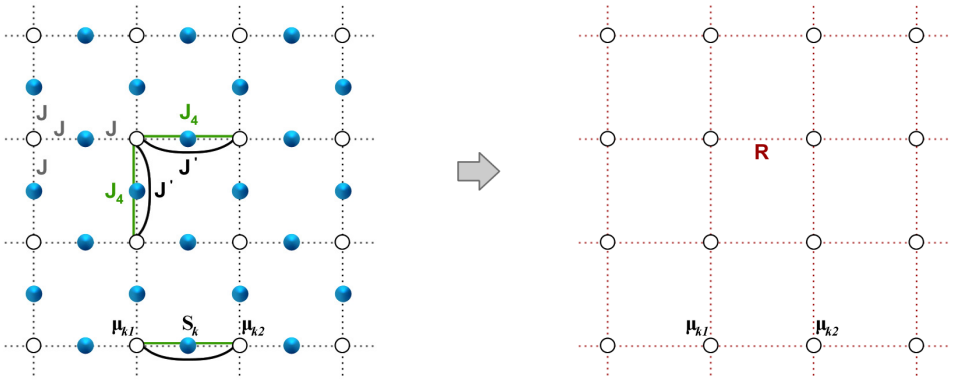

Fig. 5.1: a) The fragment of the decorated square lattice under investigation. The doted lines denote bilinear interactions J between nearest neighbors, black lines denote bilinear interactions $J^{'}$ between next- nearest neighbors and green lines indicate three-site four-spin interactions J_4. The open circles display spin-1/2 atoms creating a sublattice A and blue circles represent decorating spin-S atoms creating a sublattice B. b) The fragment of the original non-decorated square lattice.

In the previous equation $\mathcal{Z}_0(\beta R)$ represents the partition function of the spin-1/2 Ising model on the square lattice (see Fig. 5.1 b)) which has been exactly calculated in a seminal Onsager's work [118]. The parameters A and R are then given by

$$A = \sqrt{w_1 w_2}, \qquad \beta R = 2\ln\left(\frac{w_1}{w_2}\right), \tag{5.3}$$

where for spin-1 decorating atoms we have

$$w_1 = \left[1 + 2\mathrm{e}^{\beta\left(D+\frac{J_4}{4}\right)}\cosh(\beta J)\right]\mathrm{e}^{\frac{\beta J'}{4}} \tag{5.4}$$

$$w_2 = \left[1 + 2\mathrm{e}^{\beta\left(D-\frac{J_4}{4}\right)}\right]\mathrm{e}^{-\frac{\beta J'}{4}} \tag{5.5}$$

while for $S = 3/2$ one obtains

$$w_1 = 2K_1\mathrm{e}^{\frac{\beta J'}{4}}, \tag{5.6}$$

$$w_2 = 2K_2\mathrm{e}^{-\frac{\beta J'}{4}}, \tag{5.7}$$

with

$$K_1 = \mathrm{e}^{\frac{9\beta}{4}\left(D+\frac{J_4}{4}\right)}\cosh\left(\frac{3}{2}\beta J\right) + \mathrm{e}^{\frac{\beta}{4}\left(D+\frac{J_4}{4}\right)}\cosh\left(\frac{\beta J}{2}\right) \tag{5.8}$$

$$K_2 = \mathrm{e}^{\frac{9\beta}{4}\left(D-\frac{J_4}{4}\right)} + \mathrm{e}^{\frac{\beta}{4}\left(D-\frac{J_4}{4}\right)}. \tag{5.9}$$

Consequently, using the general relation (4.10) one easily gets the final equation for the Helmholtz free energy for both decorated system, namely,

$$F(\beta, J, J_4, J', D) = -2N\beta^{-1}\ln A(\beta, J, J_4, J', D) + F_0(\beta, R), \tag{5.10}$$

where parameters A, R are given by (5.3) and $F_0(\beta, R)$ represents the Helmholtz free energy of the original non-decorated Ising square lattice [118]

$$F_0(\beta, R) = -\frac{N}{\beta}\left[\ln\left(2\cosh\frac{\beta R}{2}\right) + \frac{1}{2\pi}\int_0^{\pi}\zeta(\varphi)\,d\varphi\right] \tag{5.11}$$

with

$$\zeta(\varphi) = \ln\left[\frac{1}{2}\left(1 + \sqrt{1 - \varkappa^2\sin^2\varphi}\right)\right] \tag{5.12}$$

and

$$\varkappa = \frac{2\sinh\left(\frac{\beta R}{2}\right)}{\cosh^2\left(\frac{\beta R}{2}\right)}. \tag{5.13}$$

Having obtained the Helmholtz free energy, one can now calculate the entropy, specific heat and internal energy from Eqs. (4.11) in a straightforward manner.

However, the understanding of phase transitions in the system under investigation requires the detailed knowledge of local spin ordering at the ground state and also at finite temperatures. Therefore, in addition to the global physical quantities evaluated above, we must also calculate various local correlation functions and also sublattice magnetizations.

These quantities cannot be obtained directly from the partition function, however, one can calculate them using the generalized Callen-Suzuki identities [123,124] which take the following general form

$$\langle S_k f_k \rangle = \left\langle f_k \frac{\sum_{S_k} S_k \mathrm{e}^{-\beta \mathcal{H}_k}}{\sum_{S_k} \mathrm{e}^{-\beta \mathcal{H}_k}} \right\rangle \tag{5.14}$$

$$\left\langle S_k^2 f_k \right\rangle = \left\langle f_k \frac{\sum_{S_k} S_k^2 \mathrm{e}^{-\beta \mathcal{H}_k}}{\sum_{S_k} \mathrm{e}^{-\beta \mathcal{H}_k}} \right\rangle, \tag{5.15}$$

where f_k represents a function of arbitrary spin variables except of the variable S_k and the angular brackets denote the standard canonical averaging with the density matrix $\rho = \exp(-\beta \mathcal{H}/\mathcal{Z})$. For the particular case of $S = 1$ decorating atoms one easily obtains from (5.14) and (5.15) the following equations

$$\langle S_k f_k \rangle = \left\langle f_k \frac{2 \sinh \left[\beta J(\mu_{k1} + \mu_{k2})\right]}{2 \cosh \left[\beta J(\mu_{k1} + \mu_{k2})\right] + \mathrm{e}^{-\beta(D + J_4 \mu_{k1} \mu_{k2})}} \right\rangle, \tag{5.16}$$

$$\left\langle S_k^2 f_k \right\rangle = \left\langle f_k \frac{2 \cosh \left[\beta J(\mu_{k1} + \mu_{k2})\right]}{2 \cosh \left[\beta J(\mu_{k1} + \mu_{k2})\right] + \mathrm{e}^{-\beta(D + J_4 \mu_{k1} \mu_{k2})}} \right\rangle, \tag{5.17}$$

and for the case of $S = 3/2$ decoration one gets

$$\langle S_k f_k \rangle = \left\langle f_k \frac{3 \sinh \left[\frac{3}{2}\beta J(\mu_{k1} + \mu_{k2})\right] + \mathrm{e}^{-2\beta(D + J_4 \mu_{k1} \mu_{k2})} \sinh \left[\frac{1}{2}\beta J(\mu_{k1} + \mu_{k2})\right]}{2 \cosh \left[\frac{3}{2}\beta J(\mu_{k1} + \mu_{k2})\right] + 2\mathrm{e}^{-2\beta(D + J_4 \mu_{k1} \mu_{k2})} \cosh \left[\frac{1}{2}\beta J(\mu_{k1} + \mu_{k2})\right]} \right\rangle \tag{5.18}$$

$$\left\langle S_k^2 f_k \right\rangle = \left\langle f_k \frac{9 \cosh \left[\frac{3}{2}\beta J(\mu_{k1} + \mu_{k2})\right] + \mathrm{e}^{-2\beta(D + J_4 \mu_{k1} \mu_{k2})} \cosh \left[\frac{1}{2}\beta J(\mu_{k1} + \mu_{k2})\right]}{4 \cosh \left[\frac{3}{2}\beta J(\mu_{k1} + \mu_{k2})\right] + 4\mathrm{e}^{-2\beta(D + J_4 \mu_{k1} \mu_{k2})} \cosh \left[\frac{1}{2}\beta J(\mu_{k1} + \mu_{k2})\right]} \right\rangle \tag{5.19}$$

In order to evaluate r.h.s of (5.16)-(5.19), one can apply the differential operator technique [125], [126], which is based on the following relations

$$g\left(x + \lambda_x, y + \lambda_y\right) = \mathrm{e}^{(\lambda_x \nabla_x + \lambda_y \nabla_y)} g\left(x, y\right) \tag{5.20}$$

and

$$\mathrm{e}^{a\mu} = \cosh\left(\frac{a}{2}\right) + 2\mu \sinh\left(\frac{a}{2}\right), \quad \mu = \pm\frac{1}{2}, \tag{5.21}$$

where $\nabla_x = \partial/\partial x$, $\nabla_y = \partial/\partial y$ are the standard differential operators and a stands for an arbitrary parameter. Applying (5.20) and (5.21) one rewrites Eqs. (5.16)-(5.19) in the following general form

$$\langle S_k f_k \rangle = \langle f_k(\mu_{k1} + \mu_{k2}) \rangle A_1 \tag{5.22}$$

and

$$\langle S_k^2 f_k \rangle = \langle f_k \rangle A_0 + 4 \langle f_k \mu_{k1} \mu_{k2} \rangle A_2, \tag{5.23}$$

where the coefficients $A_i = A_i(\beta, J, J_4, D)$, $i = 0, 1, 2$ take the following explicit form

$$A_0 = \frac{1}{2}\left[G\Big(J, \frac{J_4}{4}\Big) + G\Big(0, -\frac{J_4}{4}\Big) \right], \tag{5.24}$$

$$A_1 = F\left(J, \frac{J}{4}\right), \tag{5.25}$$

$$A_2 = \frac{1}{2}\left[G\Big(J, \frac{J_4}{4}\Big) - G\Big(0, -\frac{J_4}{4}\Big) \right]. \tag{5.26}$$

The functions $G(x, y)$ and $F(x, y)$ depend on the spin of decorating atoms and for $S = 1$ they are given by

$$G(x, y) = \frac{2\cosh(\beta x)}{2\cosh(\beta x) + \exp(-\beta D - \beta y)}, \tag{5.27}$$

$$F(x, y) = \frac{2\sinh(\beta x)}{2\cosh(\beta x) + \exp(-\beta D - \beta y)}, \tag{5.28}$$

while for $S = 3/2$ we have

$$G(x, y) = \frac{9\cosh\left(\frac{3}{2}\beta x\right) + \mathrm{e}^{-2\beta(D+y)}\cosh\left(\frac{1}{2}\beta x\right)}{4\cosh\left(\frac{3}{2}\beta x\right) + 4\mathrm{e}^{-2\beta(D+y)}\cosh\left(\frac{1}{2}\beta x\right)} \tag{5.29}$$

and

$$F(x, y) = \frac{3\sinh\left(\frac{3}{2}\beta x\right) + \mathrm{e}^{-2\beta(D+y)}\sinh\left(\frac{1}{2}\beta x\right)}{2\cosh\left(\frac{3}{2}\beta x\right) + 2\mathrm{e}^{-2\beta(D+y)}\cosh\left(\frac{1}{2}\beta x\right)}. \tag{5.30}$$

After substituting $f_k = 1$ into (5.22) and (5.23), we obtain equations for the evaluation of the sub-lattice magnetization m_B

$$m_B = \langle S_k \rangle = \langle \mu_{k1} \rangle A_1, \tag{5.31}$$

and the quadrupolar momentum q_B

$$q_B = \langle S_k^2 \rangle = A_0 + 4 \langle \mu_{k1} \mu_{k2} \rangle A_2. \tag{5.32}$$

Similarly, putting $f_k = \mu_{k1}$ and $f_k = \mu_{k1}\mu_{k2}$, one gets expressions for important local correlation functions, namely,

$$\langle S_k \mu_{k1} \rangle = \left(\frac{1}{4} + \langle \mu_{k1}\mu_{k2} \rangle \right) A_1, \tag{5.33}$$

$$\left\langle S_k^2 \mu_{k1} \right\rangle = \langle \mu_{k1} \rangle \left(A_0 + A_2 \right), \tag{5.34}$$

$$\left\langle S_k^2 \mu_{k1}\mu_{k2} \right\rangle = \langle \mu_{k1}\mu_{k2} \rangle A_0 + \frac{A_2}{8}. \tag{5.35}$$

The magnetization of decorating spins $m_A = \langle \mu_{k1} \rangle = \langle \mu_{k2} \rangle$ and also the correlation function $c = \langle \mu_{k1}\mu_{k2} \rangle$ appearing on the right hand side of (5.28)-(5.35) can be obtained very simply from the relation [116]

$$\langle f(\mu_{k1}, \mu_{k2}, \ldots, \mu_{ki}) \rangle = \langle f(\mu_{k1}, \mu_{k2}, \ldots, \mu_{ki}) \rangle_0 , \tag{5.36}$$

where f represents an arbitrary function depending exclusively on the spin variables of A sublattice and the symbol $\langle \ldots \rangle_0$ denotes the canonical averaging using the density matrix $\rho_0 = \exp(-\beta \mathcal{H}_0)/\mathcal{Z}_0$.

The calculation of m_A is now a rather simple task, since setting $f(\mu_{k1}, \mu_{k2}, \ldots, \mu_{ki}) = \mu_{ki}$ one obtains

$$m_A = \langle \mu_{ki} \rangle = \langle \mu_{ki} \rangle_0 = m_0, \tag{5.37}$$

where m_0 represents the magnetization per one lattice site of the original square lattice. This magnetization has been exactly calculated by Yang [127] and it is given by

$$m_0 = \frac{1}{2} \left(1 - \frac{16 e^{-2\beta R}}{\left(1 - e^{-\beta R}\right)^4} \right)^{\frac{1}{8}}. \tag{5.38}$$

The total magnetization of decorated lattice reduced per one lattice site is defined as $m = (m_A + 2m_B)/3$ and using Eq. (5.28) it can be expressed in the following simple form

$$m = \frac{1}{3}(1 + 2A_1) m_0. \tag{5.39}$$

The critical temperature of the square lattice has been exactly obtained by Onsager [118] and it given by $k_B T_c/R = \left[2 \ln\left(\sqrt{2}+1\right)\right]^{-1}$. Consequently taking into account Eq. (5.39), the finite-temperature phase boundaries of the decorated system can be evaluated by substituting this value into (5.3). Then, using Eqs. (5.4) and (5.5) one gets for the mixed spin-1/2 and spin-1 decorated system the following equation for the critical temperature:

$$2 \ln\left(\sqrt{2}+1\right) = \beta_c J' + 2 \ln \frac{1 + 2\mathrm{e}^{\beta_c (D + \frac{J_4}{4})} \cosh(\beta_c J)}{1 + 2\mathrm{e}^{\beta_c (D - \frac{J_4}{4})}}. \tag{5.40}$$

Similarly, for the mixed spin-1/2 and spin-3/2 system, we utilize Eqs. (5.6)-(5.9) and obtain the relation for critical boundary in the form

$$2 \ln\left(\sqrt{2}+1\right) = \beta_c \left(J' + \frac{9}{4} J_4 \right) + 2 \ln \frac{\cosh\left(\frac{3}{2}\beta_c J\right) + \mathrm{e}^{-2\beta_c (D + \frac{J_4}{4})} \cosh\left(\frac{1}{2}\beta_c J\right)}{1 + 2\mathrm{e}^{-2\beta_c (D - \frac{J_4}{4})}}, \tag{5.41}$$

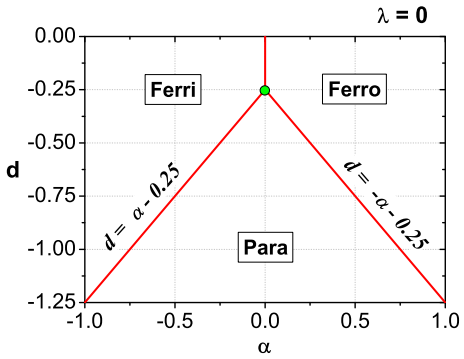

Fig. 5.2: Ground-state phase diagram in the $\alpha - d$ space for the mixed-spin Ising model without next-nearest pair interaction ($\lambda = 0$). Copyright © 2016 Elsevier.

with $\beta_c = 1/(k_B T_c)$. Moreover, it is clear from the general expression for the Helmholtz free energy (5.10) that the contribution of decorating atoms to the total Helmholtz free energy is represented by an analytic function in the whole parameter space. Therefore the critical behavior of all decorated Ising models will necessarily belong to the same universality class as that one of the usual 2D Ising model.

Finally, it is worth noticing that if one alternatively calculates the internal energy of the systems as $U = \langle \mathcal{H} \rangle$, then it can be expressed in the form

$$\frac{U}{2N} = -J\big\langle(\mu_{k1}^z + \mu_{k2}^z)S_k^z\big\rangle - J'\big\langle\mu_{k1}^z\mu_{k2}^z\big\rangle - J_4\big\langle\mu_{k1}^z(S_k^z)^2\mu_{k2}^z\big\rangle - D\big\langle(S_k^z)^2\big\rangle, \qquad (5.42)$$

which will be used in the forthcoming text for determination ground-state boundaries for both $S = 1$ and $S = 3/2$ cases.

5.2 Numerical results for the mixed spin-1/2 and spin-1 decorated model

In this part we will review results presented recently in [120, 121] for the model with spin-1 decorated atoms and for this purpose we introduce the following dimensionless parameters: $\alpha = J/J_4$, $\lambda = J'/J_4$ and $d = D/J_4$.

5.2.1 Ground-state phase diagram

In order to investigate the physical nature of possible phases at the ground state, one has numerically investigate the sub-lattice magnetizations, quadrupolar moment and various correlations functions in our system at $T = 0$. On the basis of these calculations, the ground-state phase boundaries can be established from the minimum values of the internal energy (5.42). In Fig in Fig. 5.2 the ground-state phase diagram is shown in the $\alpha - d$ space for the special case of $\lambda = 0$, i.e. $J' = 0$,.

At first here will be discussed the particular case of the system with pure three-site interaction i.e., with $\alpha = \lambda = 0$. As it follows from Eqs. (5.28) and (5.37), in this case the sublattice magnetization m_B becomes zero for arbitrary values of d and the same statement applies also for all correlations including one spin of B sublattice. In addition, one finds from Eq.(5.32) that the quadrupolar moment $\langle S_k^2 \rangle = 1$ for $d > -0,25$, thus the spin states $S_k = +1$ and $S_k = -1$ of all decorating atoms are equally likely occupied at $T = 0$, while the sublattice A exhibits the long-range order with $m_A = 1/2$. Consequently, such a system will exhibit the non-zero ground-state entropy $S_0/N = k_B \ln 4 \doteq 1.386 k_B$ originated from the disorder on B sublattice. This is a rather surprising behavior, which appears as a result of the competition between three-site interaction J_4 and crystal-field parameter D. On the other hand, for $\alpha = 0$ and $d < -0.25$ we easily obtain from (5.32) $\langle S_k^2 \rangle = 0$ indicating that $m_B = 0$, since all decorating atoms occupy the spin states $S_k = 0$. In this case each atom on the A sublattice is surrounded by decorating atoms with $S_k = 0$, so that all atoms of the A sub-lattice can be found equally likely in the spin state $\mu_{kj} = +1/2$ or $\mu_{kj} = -1/2$. Subsequently, the entropy at $T = 0$ will now take the value $S_0/N = k_B \ln 2 \doteq 0.693 k_B$ and in this case no magnetic order appears in the ground state.

The most surprising behavior of system we have found at the point with coordinates $\alpha = 0$ and $d = -0.25$, where a very interesting partially ordered phase with $m_B = 0$, $\langle S_k^2 \rangle \doteq 0.642$ and non-saturated value $m_A \doteq 0.476$ has been observed. This special magnetic phase has unusually high value of the ground state entropy, $S_0/N \doteq 2.213 k_B$, and as far as we know, such a phase has been reported only very recently [121].

As one can see from the Fig 5.2, for $\alpha \neq 0$ three standard phase can be stable in the system depending on the value of the crystal field parameter. Namely, the ordered ferrimagnetic phase becomes stable in the region above the line $d = \alpha - 0.25$ for negative values of the nearest-neighbor pair exchange interaction ($\alpha < 0$). On the other hand, for $\alpha > 0$ the ferromagnetic ordering appears in the region above the line $d = -\alpha - 0.25$. These two lines terminate at $d = -0.25$ and for $d > -0.25$ the ordered ferrimagnetic or ferromagnetic phase is respectively stable for arbitrary negative or positive values of α.

Next it follows from the Fig. 5.2 that the disordered paramagnetic phase becomes stable in the ground state for arbitrary values of α whenever the crystal-field parameter d satisfies inequality $d < -|\alpha| - 0.25$. Thus the magnetic order can be always destroyed taking the value of single-ion anisotropy negative and strong enough. Along the boundary lines $d = -|\alpha| - 0.25$, the ordered phases can coexist with the paramagnetic one and the system may exhibit a first-order phase transition when crossing this line.

Now, let us briefly mention the effect of a positive next-nearest-neighbor interaction, i.e. $\lambda > 0$. Any positive bilinear exchange interaction supports ferromagnetic ordering of spins on the A sublattice and therefore in this case the disordered paramagnetic phase never becomes stable at $T = 0$. Thus, for $\alpha > 0$ the system will always exhibit the long-range order with $(m_A, m_B) = (1/2, 1)$ and $(m_A, m_B) = (1/2, -1)$ for $\alpha < 0$. The situation for $\alpha = 0$, $d > -0.25$ and $\lambda > 0$ becomes identical with the above discussed case with $\alpha = 0$, $d > -0.25$ and $\lambda = 0$. Finally, for $\alpha = 0$, $d < -0.25$ and $\lambda > 0$, the system will exhibit a long-range order on the A sublattice, despite of the fact that all atoms of the B sub-lattice will occupy the zero-spin states. However, contrary to the case with $\lambda = 0$, the entropy of the system now always vanishes in the limit of $T \to 0$. To avoid confusing, one should notice that all the mixed phases, i. e., partially ordered phases appearing along the lines $\alpha = 0$ and $d = \pm\alpha - 0.25$, should be regarded as new separate phases of the system.

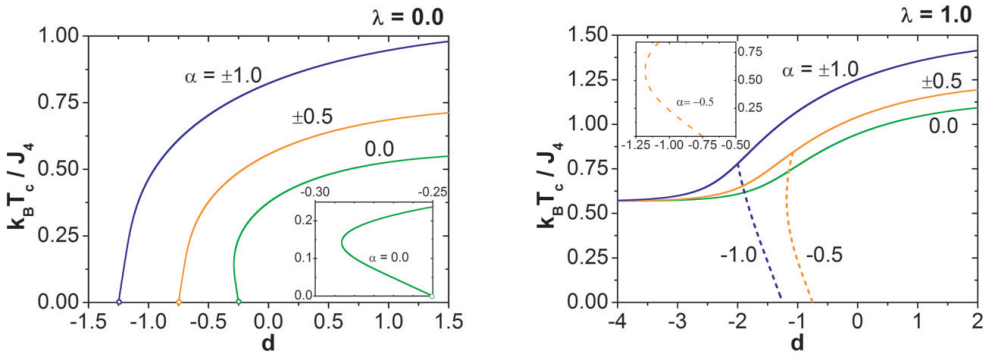

a) b)

Fig. 5.3: (a) Phase diagrams of the decorated mixed-spin Ising system in the $d - T_c$ space for $\lambda = 0$ and several typical values of α. The insert shows the detail view for $\alpha = 0.0$ with re-entrant behavior retaining two critical temperatures. Copyright © 2016 Elsevier.
(b) The same as in case (a) but for $\lambda = 1$. The critical boundaries are depicted by full lines and compensation temperatures by dashes ones. The insert shows a possibility of two compensation temperatures in a narrow region of negative values of d. Copyright © 2016 Elsevier.

5.2.2 Finite temperature phase diagrams

In section 5.1 it has been shown that the critical temperature of the mixed spin1/2 and spin-1 decorated system can be calculated from (5.40) and since this equation is invariant under changing the sign of parameter J then both ferromagnetic ($J > 0$) and ferrimagnetic ($J < 0$) phases will exhibit the same critical temperature. In addition to the critical temperature, it is also interesting to investigate the compensation temperature which is defined as a temperature at which the total magnetization vanishes below the critical temperature, so that is our case it is determined by the condition $m = (m_A + 2m_B) = 0$. This temperature is, of course, relevant only for the ferrimagnetic ordering, i.e., for $J < 0$). The characteristic phase boundaries in the $T_c - d$ plane are for $|\alpha| = 0,\ 0.5$ and 1 depicted in Fig. 5.3a) for $\lambda = 0.0$ and in Fig. 5.3b) for $\lambda = 1.0$. As one can see from the figures, all critical curves are really independent of the sign of the nearest-neighbor interaction, so that both the ferromagnetic $(m_A > 0, m_B > 0)$ and ferrimagnetic $(m_A > 0, m_B < 0)$ phases always vanish at the same critical temperature. The presented results are naturally in agreement with the analysis of ground state in the previous section. Indeed, as one can see from Fig. 5.3a), the ordered phase is for $\lambda = 0.0$ stable at the ground state only for $d > -|\alpha| - 0.25$, while outside of this region (i.e., for negative and strong enough values of d), the system becomes disordered at all temperature including the case $T = 0$. As one can expect, for $d > -|\alpha| - 0.25$ the magnetization will gradually decrease with the increasing temperature, until it will continuously vanish at some critical temperature T_c. The system under investigation obviously undergoes the conventional second-order phase transition from the ordered (ferrromagnetic or ferrimagnetic) phase to disordered paramagnetic phase when crossing the relevant

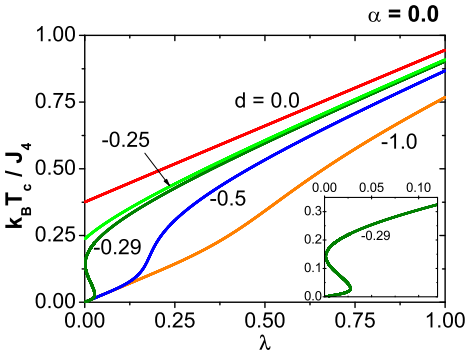

Fig. 5.4: Phase diagrams of the decorated mixed-spin Ising system in the $\lambda - T_c$ space for $\alpha = 0$ and several typical values of d. The inset shows the detail view for $d = -0.29$ when appears a re-entrant behavior with three critical temperatures. Copyright © 2016 Elsevier.

phase boundary. As we have already mentioned above, all such phase transitions in decorated Ising spin systems are of the second-order and belong to the 2D Ising universality class.

Finally, the special case of the system with the pure three-site four-spin interaction will be inspected. In this case, the partially ordered phase with $m_A \neq 0$ and $m_B = 0$ is stable bellow T_c for $d > -0.25$, while the standard paramagnetic phase becomes stable above the critical temperature. Moreover, one observes the C-shaped form of critical boundary in a narrow low-temperature region in the neighborhood of $d = -0.25$. This dependence implies a possibility of re-entrant behavior with two phase transitions within the indicated region (see the insert in Fig. 5.3a). We recall that for the particular choice of $\lambda = 0$ discussed above, we have never observed the existence compensation points in decorated system under investigation.

On the other hand, as one can expect, the situation will significantly change by setting non-zero next-nearest-neighbor pair interaction, i.e., $\lambda \neq 0$. A positive value of the parameter λ eliminates the existence of the paramagnetic phase at $T = 0$, regardless of the values of other parameters and it also significantly supports ordering on the A sublattice, so that compensation phenomenon may appear in the system. The situation is shown in Fig. 5.3 b), where by the full lines some typical phase boundaries are shown for $\lambda = 1.0$ and the same values of α as in Fig. 5.3 a). One can see from the figure, that the ground state of the system never becomes fully disordered, as it also follows from the discussion in previous subsection.

The compensation effect is only possible for relatively strong nonzero values of λ, because to get this effect it is necessary to keep the sub-lattice magnetization m_A strong enough over a large temperature region. Several typical dependencies of the compensation temperature on the parameter d are depicted in Fig. 5.3 b) by dashed lines for $\lambda = 1.0$, $\alpha = -1.0$ and $\alpha = -0.5$. Moreover, the insert in this figure indicates that even two compensation temperatures are possible in a narrow region of the negative values of d. As far as we know, such a finding for the systems with the higher-order spin interactions has been first time reported very recently in [121].

In order to illustrate the influence of non-zero parameter λ on the re-entrant behavior of the system, the phase boundaries in the $\lambda - T_c$ space are depicted in Fig. 5.4 for $\alpha = 0$. As it is

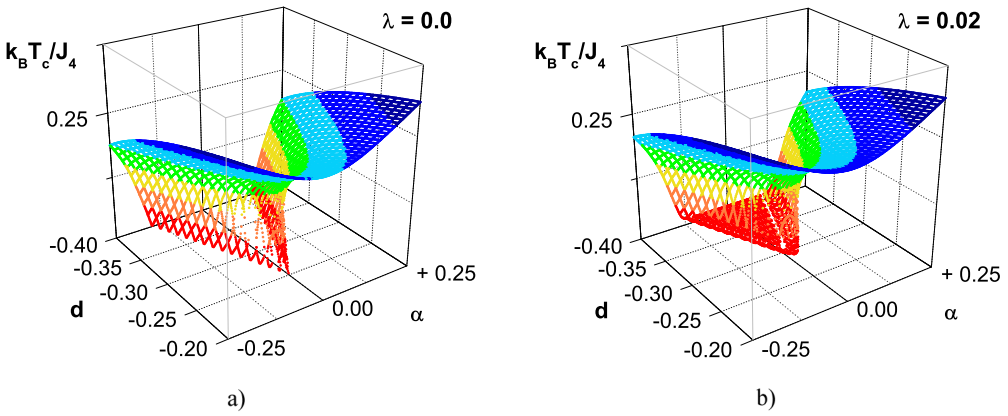

Fig. 5.5: Global phase diagrams of the decorated mixed-spin Ising system in the $d-\alpha-T_c$ space for $\lambda = 0$ (a) and $\lambda = 0.02$ (b).

clearly visible, even a re-entrant behavior with three different critical temperatures may appear in the system for modest values of λ, if the crystal field parameter is selected in the neighborhood of $d \approx -0.3$.

Finally, to show a global view of the critical surface the three-dimensional phase diagrams of the system under investigation are presented in Figs. 5.5 a) and 5.5b) for $\lambda = 0$ and $\lambda = 0.02$, respectively.

5.2.3 Magnetization, entropy and specific heat

In this part we will support our previous discussion by the analysis of temperature dependencies of relevant physical quantities. At first, in Figs. 5.6a) and 5.6b) there are shown thermal variations of the sublattice magnetization m_A and the quadrupolar moment q_B for $\alpha = \lambda = 0$ and some typical values of d. Let us recall that the sublattice B does not exhibit the long-range order, since the magnetization m_B vanishes for arbitrary values of d and the temperature, whenever is $\alpha = 0$. Subsequently, at $T = 0$ the system as a whole will be partially ferromagnetically ordered for $d > -0.25$ with $m_A = 0.5,\ m_B = 0$ and $q_B = 1$. This situation is illustrated in Figs. 5.6a) and 5.6 b) choosing $d = -0.24,\ 0$ and 1.0. On the other hand, for $\alpha = \lambda = 0$ and $d = -0.25$ one finds that instead of the saturation value, the sublattice magnetization takes the value $m_A = 0.475$, while the quadrupolar moment $q_B = 0.642$. These values indicate that both sublattices exhibit very interesting frustrated behavior which originates from the competition between the three-site four-spin interaction and crystal field. As far as we know, such a finding has been for the Ising models first time reported in [121]. Next, if one selects the value of d slightly bellow $d = -0.25$, then one finds find a reentrant behavior in the temperature behavior of the magnetization m_A as it is shown in Fig 5.6a) for $d = -0.265$. In this case, the stability of paramagnetic phase extends down to zero temperature, since it has the lowest Helmholtz free energy in the relevant temperature range.

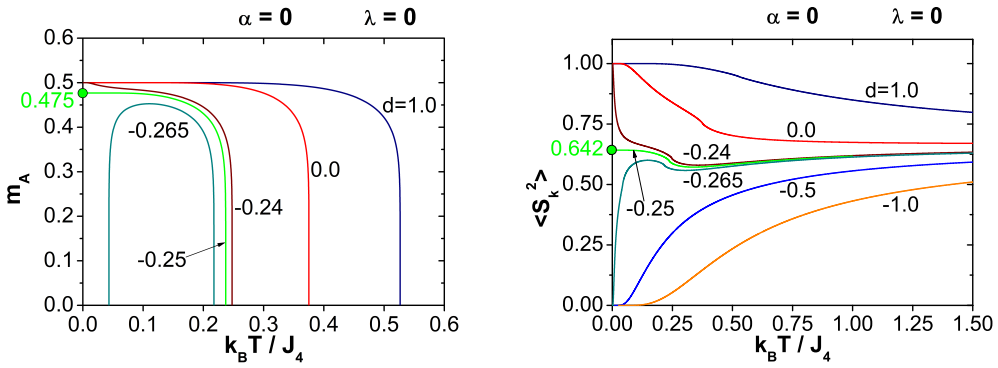

a) b)

Fig. 5.6: (a) Thermal dependencies of sub-lattice magnetization m_A and (b) quadrupolar momentum $\langle (S_k^z)^2 \rangle$ of the decorated mixed-spin Ising system for $\alpha = \lambda = 0.0$ and several typical values of d. Copyright © 2016 Elsevier.

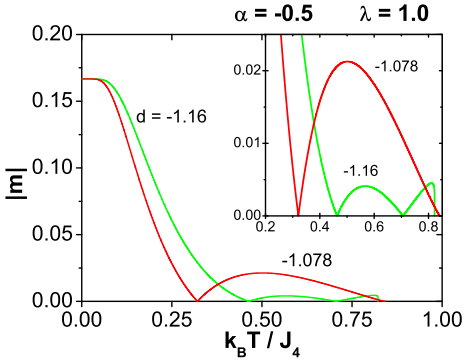

Fig. 5.7: Temperature dependencies of the absolute value of total magnetization per spin. The existence of both one and two compensation temperatures are illustrated. Copyright © 2016 Elsevier.

According to the results presented in Fig. 5.3b) for $\lambda = 1.0$, very interesting thermal variations of the magnetization may be found for the ferrimagnetic case (i.e., $\alpha < 0$) in the region where compensation effects take place. To illustrate such a behavior, the magnetization curves exhibiting one (the red curve) or two compensation temperatures (the green curve) are shown in Fig. 5.7.

Next it is also of interest to investigate the system with pure three-site four-spin interaction which exhibits finite values of entropy in the ground state. In order to confirm this unexpected

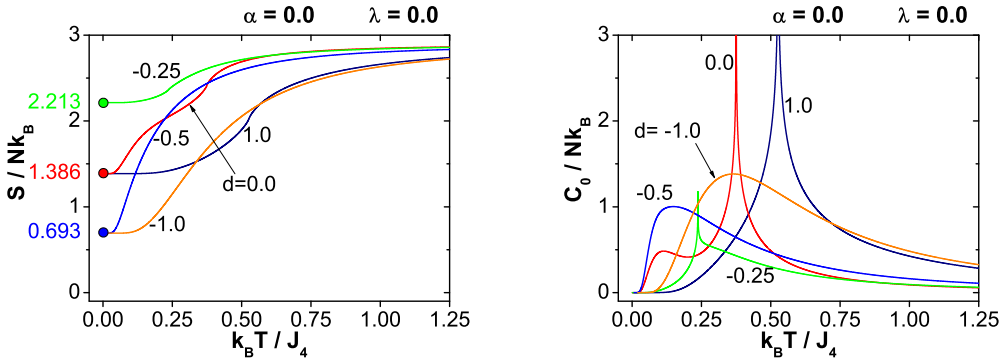

Fig. 5.8: (a) Thermal dependencies of reduced entropy of the decorated mixed-spin Ising system for $\alpha = \lambda = 0.0$ and several typical values of d. Copyright © 2016 Elsevier. (b) Thermal dependencies of reduced specific heat of the decorated mixed-spin Ising system for $\alpha = \lambda = 0.0$ and the same values of d as in case a). Copyright © 2016 Elsevier.

behavior, the temperature dependencies of entropy are depicted in Fig. 5.8 a) for $\alpha = \lambda = 0$ and several values of d corresponding to Figs. 5.6 a) and 5.6 b). The presented results clearly demonstrate that the ground-state entropy of the system may take three different values depending on the value of d, namely,

$$\begin{aligned} S_0 &= Nk_B \ln 2 \approx 0.693 Nk_B \qquad \text{for } d < -0.25 \\ S_0 &= 2Nk_B \ln 2 \approx 1.386 Nk_B \qquad \text{for } d > -0.25. \\ S_0 &\approx 2.213 Nk_B \qquad \text{for } d = -0.25. \end{aligned} \tag{5.43}$$

Here one should emphasize that the value of $S_0 \approx 0.693 Nk_B$ originates solely from the contribution of the A sublattice, while the second non zero value of $S_0 \approx 1.386 Nk_B$ represents exclusive contribution of the B sublattice. Both these values correspond to the spin configurations described in detail within discussion of the ground-state phase diagram. On the other hand, the value of entropy $S_0 = 2.213 Nk_B$ for $d = -0.25$ cannot be ascribed to the one sublattice only. In fact, the total value consists of two different contributions. i.e., $S_0 = S_{0B} + S_{0A}$, where the major contribution S_{0B} comes from the B sublattice in which all three spin states $S_i^z = 0, \pm 1$ are at $T = 0$ randomly occupied (see the green curve in Fig. 5.8a). The second contribution S_{0A} comes from the A sublattice which is also slightly disordered at $T = 0$. This fact is clearly illustrated by the green curves in Figs. 5.6a) and 5.6b) which do not reach their saturated values at $T = 0$.

Finally, it is also useful to study the temperature dependencies of the magnetic specific heat. The results of the specific heat obtained for a special case of $\alpha = 0$, $\lambda = 0$ are presented in Fig. 5.8b). As one can see from the figure, the curves for $d = 1.0$, 0.0 and $-0,25$ exhibit at critical point the same singularity as the standard spin-1/2 Ising model on a square lattice. Similarly, for strong negative values of d one observes the expected behavior for the paramagnetic

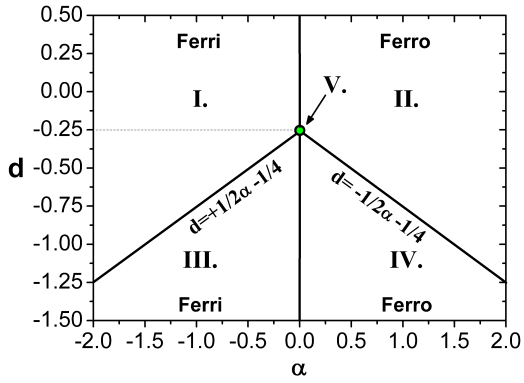

Fig. 5.9: The ground-state phase diagram in $\alpha - d$ space for $\lambda = 0$. Regions I. - V. denote phases with different spin configuration. Copyright © 2017 Elsevier.

systems. One should emphasize here that despite of non-zero ground-state entropy (see Fig. 5.8 a)), the specific heat goes always to zero for $T \to 0$, in agreement with the Third Law of Thermodynamics.

5.3 Numerical results of mixed spin-1/2 and spin-3/2 Ising spin system with three-site four-spin interaction on square lattice

In this part we will continue with the discussion of numerical results for bond-decorated Ising model on a square lattice consisting of nodal atoms with spin 1/2 and decorating atoms with spin 3/2 [122]. Calculations follows directly from relevant equations presented in Sec. 5 and for the convenience of analysis we again introduce the following dimensionless parameters $\alpha = J/J_4$, $d = D/J_4$, $\lambda = J'/J_4$.

5.3.1 Ground-state phase diagram

Similarly as in in the case of spin-1 decorating atoms, also for the current system it is necessary at first to investigate the internal energy of all relevant spin configurations at $T = 0$ (see Fig. 5.10) and then construct the phase diagram in $\alpha - d$ plane. The representative ground-state phase diagram is depicted in Fig. 5.9 and one should emphasize that this phase diagram is valid for arbitrary values of the parameter λ. As one can see from the figure, in different regions of parameter space there are stable the following different ordered magnetic phases:

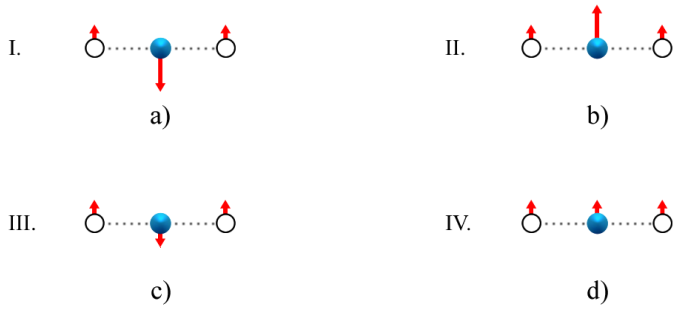

Fig. 5.10: The ground state spin configurations in the phases a) I., b) II., c) III., d) IV.

I. ferrimagnetic phase with $m_A = +\frac{1}{2}$, $m_B = -\frac{3}{2}$ $q_B = \frac{9}{4}$ for $\alpha < 0$ $d > \frac{\alpha}{2} - \frac{1}{4}$,

II. ferromagnetic phase with $m_A = +\frac{1}{2}$, $m_B = +\frac{3}{2}$ $q_B = \frac{9}{4}$ for $\alpha > 0$ $d > -\frac{\alpha}{2} - \frac{1}{4}$,

III. ferrimagnetic phase with $m_A = +\frac{1}{2}$, $m_B = -\frac{1}{2}$ $q_B = \frac{1}{4}$ for $\alpha < 0$ $d < \frac{\alpha}{2} - \frac{1}{4}$,

IV. ferromagnetic phase with $m_A = +\frac{1}{2}$, $m_B = +\frac{1}{2}$ $q_B = \frac{1}{4}$ for $\alpha > 0$ $d < -\frac{\alpha}{2} - \frac{1}{4}$.

The boundaries between various phases represent the lines of first-order phase transitions along which relevant couples of phases may co-exist. Let us at first investigate the case of pure three-site four spin interaction, i.e. $\alpha = 0$. It follows from the analysis of sublattice magnetizations and relevant correlation functions that each decorating atom occupies equally likely $\pm 3/2$ or $\pm 1/2$ spin states, respectively. Subsequently, for $\alpha = 0$ and $d > -1/4$ one finds $m_A = 1/2, m_B = 0$ and $q_B = 9/4$, while for $\alpha = 0$ and $d < 1/4$ we have $m_A = 1/2, m_B = 0$ and $q_B = 1/4$. Finally, at the special point with co-ordinates (α, d) = (0, -1/4) all four ordered phases coexist, so that the minimum of the internal energy corresponds to the partially ordered phase with $m_A = 1/2, m_B = 0$ and $q_B = 5/4$. In this case, all the states $S_k = \pm 1/2, \pm 3/2$ on B sublattice are occupied equally likely. Here one should notice that the disorder observed along the phase boundary $\alpha = 0$ will naturally lead to non-zero values of the entropy at the ground state.

The situation along two others phase boundaries is simpler, since for $d = \alpha/2 - 1/4$ and $\alpha < 0$ we have found the phase with $m_A = 1/2, m_B = -1$ and $q_B = 5/4$, while for $d = -\alpha/2 - 1/4$ and $\alpha > 0$, one finds $m_A = 1/2, m_B = 1$ and $q_B = 5/4$.

5.3.2 Critical and compensation temperatures

Having obtained the ground-state phase diagram, one can now proceed with the investigation of the system at finite temperatures. As an initial step in this direction, the critical and compensation temperatures for several representative combinations of model parameters will be analyzed.

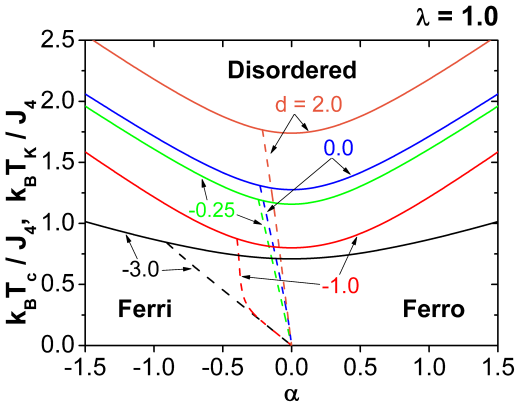

Fig. 5.11: The critical (solid curves) and compensation temperatures (dashed curves) in $\alpha - T$ space for $\lambda = 1.0$ and different values of d. Copyright © 2017 Elsevier.

The typical phase boundaries in $\alpha - T_c$ space are depicted in Fig. 5.11 for $\lambda = 1.0$ and several representative values of the single-ion anisotropy parameter d. The solid and doted curves in the figure correspond to critical and compensation temperatures, respectively. As one can see, the standard ferri- or ferromagnetic phases appear in the system at low temperatures for $\alpha < 0$ or $\alpha > 0$, respectively, while the paramagnetic phase becomes naturally stable in the high-temperature region, i.e., above each phase boundary. Consequently, in agreement with the ground-state phase diagram, the normalized spontaneous magnetization of these phases will take its saturation value at $T = 0$ and then it will gradually decrease with increasing temperature until it continuously vanishes at the corresponding critical temperature.

Next, one can also notice that for fixed values of λ the compensation phenomenon appears for all selected values of d, if we choose appropriate negative values of the parameter α. Investigating phase boundaries also for other sets of parameters one observes that independently of the values of d and λ, the relevant curves always exhibit a symmetric U-shape form with minimum values at $\alpha = 0$. Intuitively one can simply understand this minimum value of T_c, since for arbitrary combinations of model parameters, the system is for $\alpha = 0$ always ordered only partially and therefore it is easier to destroy the long-range order than in the case of in the fully ordered ferrimagnetic or ferromagnetic phases. Next, it is also of interest to study the phase diagrams in $\lambda - T$ space with the aim to clarify the influence of the next-nearest-neighbor bilinear interaction on critical and compensation temperature.

Some typical results are depicted in Fig. 5.12 for $|\alpha| = 0.1$ and several characteristic values of the parameter d. As one should expect, all phase boundaries exhibit almost a perfect linear increase with the increasing strength of the parameter λ. On the other hand, the compensation phenomenon appears for $\alpha = -0.1$ and all selected values of d and we can see that the compensation temperature does not depend on the next-nearest-neighbor bilinear interaction at all. Finally, one should also investigate the critical and compensation temperatures in $d - T_c$ space. The results are shown in Fig. 5.13 and one can see that the phase boundaries have very similar

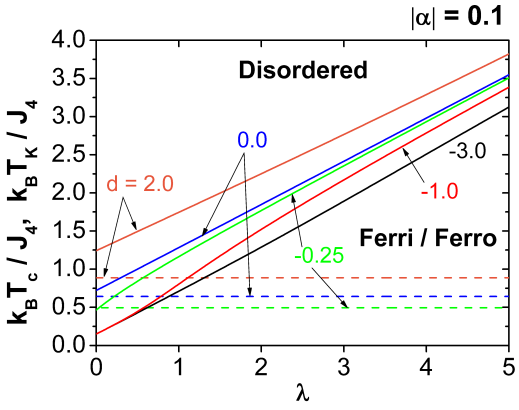

Fig. 5.12: The critical (solid curves) and compensation temperatures (dashed curves) in $\lambda - T$ space for $|\alpha| = 0.1$ and different values of d. The critical boundaries are identical for ferromagnetic ($\alpha = 0.1$) and ferrimagnetic ($\alpha = -0.1$) cases, while the compensation temperatures occure only for ferrimagnetic phase ($\alpha = -0.1$). Copyright © 2017 Elsevier.

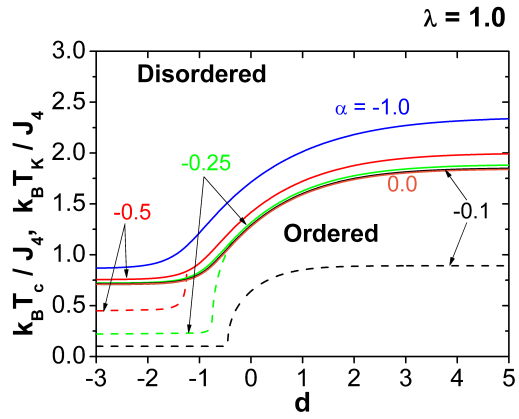

Fig. 5.13: The critical (solid curves) and compensation temperatures (dashed curves) in $d - T$ space for $\lambda = 1.0$ and different values of α. Copyright © 2017 Elsevier.

shapes as the phase diagram of standard spin-3/2 Blume-Capel model [126]. Obviously, the positive values of d promote the spin states $\pm 3/2$, while the negative values prefer the occupation of $\pm 1/2$ spin states of decorating atoms. One should emphasize here that such a behavior of spins on the B sublattice has the principal influence on the three-site four-spin exchange interaction. Since this term takes the form of $-J_4 S_k^2 \mu_{k1} \mu_{k2}$, then one simply finds that at the ground state this three-site term reduces to $-9J_4 \mu_{k1} \mu_{k2}/4$ or $-J_4 \mu_{k1} \mu_{k2}/4$ for $d \to \infty$ or $d \to -\infty$, respec-

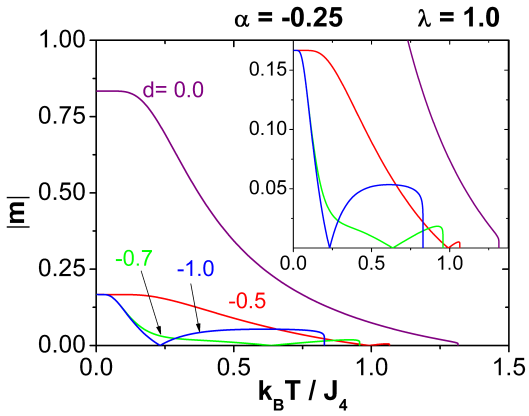

Fig. 5.14: Thermal variations of the absolute value of total magnetization per spin for $\alpha = -0.25$, $\lambda = 1.0$ and several characteristic values of the parameter d. Copyright © 2017 Elsevier.

tively. Therefore for strong values of the crystal field, the three-site four-spin interaction acts as an effective n.n.n pair interaction which substantially reinforces the influence of parameter λ and consequently keeps high values of the sublattice magnetization m_A even at higher temperature region. In particular, due to this interesting effect of the crystal field, the compensation temperatures may exist in very large regions of d and they can exhibit very interesting behavior. Indeed, the compensation temperature always takes its saturation value for $d \to -\infty$ and it very slowly increases with increasing the crystal-field parameter for arbitrary non-zero λ and some appropriate values of α (see Fig. 5.13). On the other hand, the change of relevant compensation curves becomes more dramatic in the region of $d > -2.0$, where for $\alpha < -0.211$ each compensation temperature terminates at the relevant critical boundary, while for $\alpha > -0.211$ the compensation temperatures may exist even for very strong positive values of the crystal-field parameter.

5.3.3 Magnetization, entropy, specific heat and free energy

The detailed investigation of critical and compensation temperatures in previous text has uncovered several interesting physical phenomena that may exhibit our decorated system due to the presence of unconventional three-site four-spin interaction. To put further insight on thermodynamic properties of the system under investigation, one should also discuss thermal variations of the magnetization, correlation functions, entropy, specific heat and Helmholtz free energy. One of the most interesting thermal variations of the magnetization pertains to the ferrimagnetic case with the existence of compensation points at finite temperatures. To illustrate such a behavior, several temperature dependencies of the absolute value of total magnetization per one atom are depicted in Fig. 5.14 choosing suitable values of all relevant parameters. As one can see the curves corresponding to negative value d exhibit compensation temperature, while for $d = 0.0$ no compensation appears. These results are in perfect correspondence with those presented in Figs. 5.11-5.13. Here one should mention that the investigation of compensation temperatures is

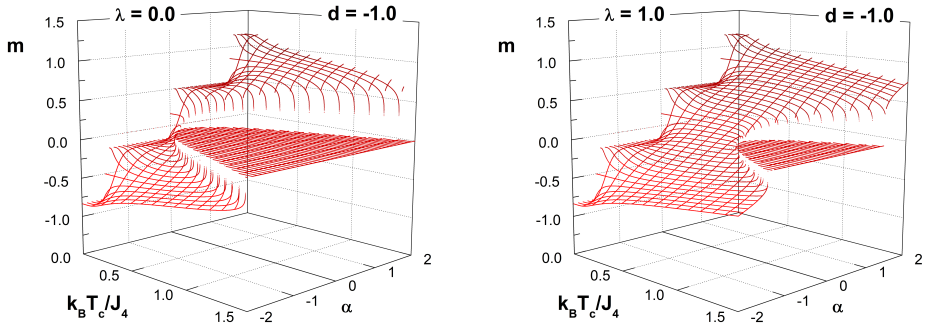

a) b)

Fig. 5.15: $T-\alpha$ dependence of the total magnetization per spin for $d=-1$ and a) $\lambda=0$, b) $\lambda=1$.

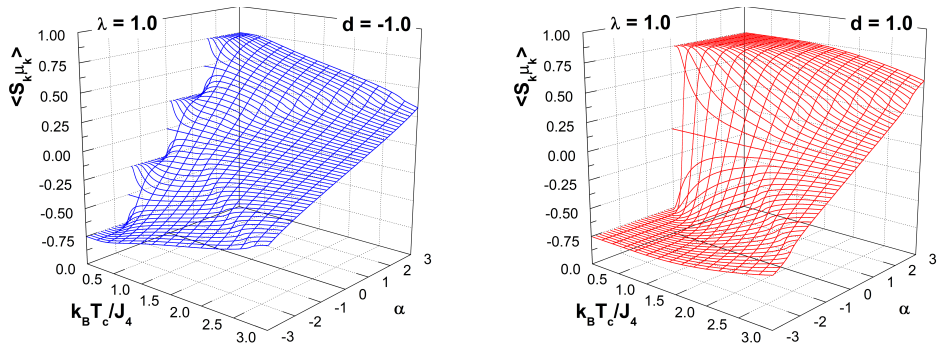

a) b)

Fig. 5.16: $T-\alpha$ dependence of the correlation function $\langle S_k\mu_k\rangle$ a) for $d=-1$ and b) for $d=1$. For both cases $\lambda=1$.

also of interest in connection with possible applications in development of new magnetic recording media. In Figs.5.15 a) and b) there are shown the dependencies of magnetization on T and α for $d=-1.0$ and $\lambda=0$ and $\lambda=1$, respectively. In accordance to the ground-state phase diagram (see Fig. 5.9) one observes seven different ground state levels of magnetization. These different magnetization levels originate from the fact that for various combinations of parameters, the minimum value of the internal energy corresponds to different spin configurations at $T=0.0$.

To support this statement, the correlation functions $\langle S_k\mu_k\rangle$, $\langle S_k^2\mu_{k1}\mu_{k2}\rangle$ and quadrupolar moment $\langle S_k^2\rangle$ as a function of T and α are, respectively, depicted in Figs. 5.16 and Fig. 5.17 for $\lambda=1.0$, $d=-1$ and 1.0. The presented dependencies of correlation functions provide the complete information about spin configurations within each local bond which is described by the

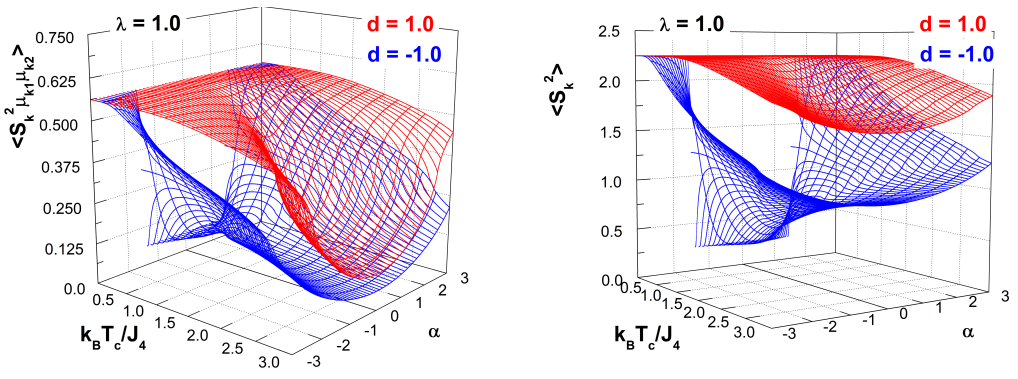

a) b)

Fig. 5.17: a) Temperature dependence of the correlation function $\langle S_k^2 \mu_{k1} \mu_{k2} \rangle$ and b) quadrupolar moment $\langle S_k^2 \rangle$. In both cases $\lambda = 1$ and $d = -1.0$ or 1.0.

bond Hamiltonian (4.19), while the quadrupolar moment describes the occupation of the $\pm 1/2$ and $\pm 3/2$ spin states on the B sublattice. One should notice here, that the comparison of results for $d = -1$ with those for $d = 1$ indicates that the role of the crystal field parameter in the systems with three-site four-spin interaction is significantly reinforced in comparison with the standard Blume-Capel models on decorated lattices [128].

Similarly as in the case of spin-one decorated model studied in previous section, also for the current system with $S = 3/2$ exhibits very interesting behavior for the special case of $\alpha = 0$, i.e., the systems with pure three-site four-spin interaction. As we have already discussed above, in this particular case the sublattice B remains strongly disordered down to zero temperature, while the sublattice A exhibits the standard long-range order at $T = 0$.

Subsequently, the system as a whole will be partially ordered with some non-zero entropy at the ground state and moreover this picture remains unchanged even for arbitrary non-negative λ. In order confirm this behavior, thermal variations of the entropy for $\alpha = 0$ and $\lambda = 1.0$ and several typical negative and positive values of d are presented in Fig. 5.18. As one can see from the figure, for $d = -0.25$ one observes $S/Nk_B = \ln(2^4) = 2.7726$, while for all other values of $d \neq -0.25$ one finds $S/Nk_B = \ln(2^2) = 1.3863$. These values correspond to the co-existence of four and two ground-state phases, respectively, and they are in a perfect agreement with the ground-state phase phase diagram (see Fig. 5.9).

Next, in order to illustrate the influence of both bilinear interactions on magnetic properties of the system, the temperature variations of entropy for $\alpha = \pm 1$, $\lambda = 1.0$ and some generic values of d are shown in Fig. 5.19. As one can see, the only non-zero value of the entropy appears now for $d = -0.75$, that corresponds to the ground-state phase point located exactly on the line given by the equation $d = \pm 0.5\alpha - 0.25$. Moreover, one also observes that the entropy does not depend on the sign of parameter α, thus the system takes exactly the same values of entropy for the ferromagnetic as well as for the ferrimagnetic equilibrium thermodynamic states for arbitrary fixed values of λ and d.

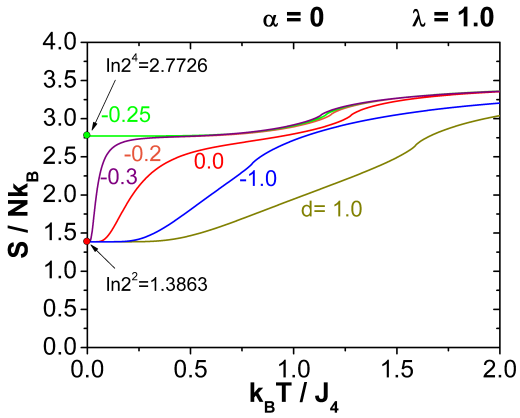

Fig. 5.18: Thermal variations of the reduced magnetic entropy for $\alpha = 0$, $\lambda = 1.0$ and several characteristic values of the parameter d. Copyright © 2017 Elsevier.

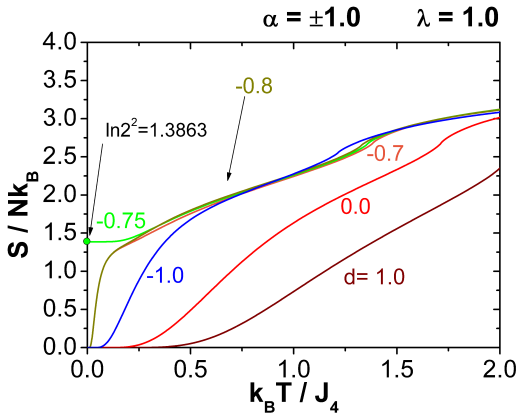

Fig. 5.19: Thermal variations of the reduced magnetic entropy for $\alpha = \pm 1$, $\lambda = 1.0$ and several characteristic values of the parameter d. Copyright © 2017 Elsevier.

To complete the investigation of thermal properties of our system, one has to calculate the magnetic part of the specific heat. Several interesting results for thermal variations of the specific heat are shown in Fig. 5.20. Here one can notice that all curves exhibit Onsager type singularity at the corresponding critical temperature and moreover, for $T \to 0$ all curves go to zero in agreement with the Third Law of Thermodynamics. It has been also observed that the specific heat exhibits for some combinations of parameters a local maximum in the low- temperature region. This broad maximum appears always, whenever the relevant set of parameters is selected from the close neighborhood of ground-state phase boundaries. In such a case the relevant spin

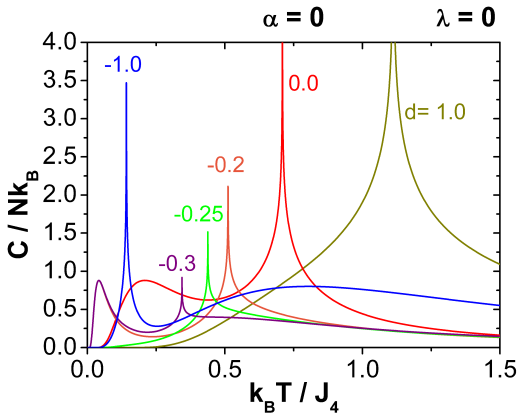

Fig. 5.20: Temperature dependencies of the reduced magnetic specific heat for $\lambda = 0$ and several characteristic values of the parameter d at a) $\alpha = 0$ and b) $\alpha = \pm 1$. Copyright © 2017 Elsevier.

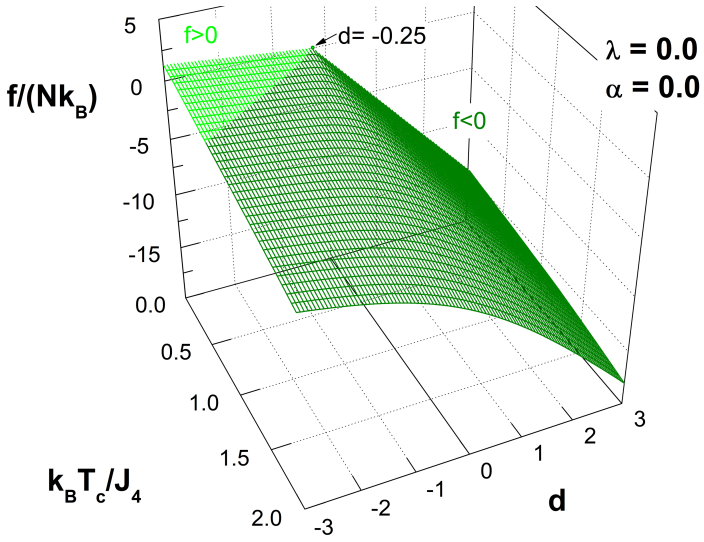

Fig. 5.21: $T - d$ dependence of the z Helmholtz free energy for the case $\lambda = 0$ and $\alpha = 0$.

states are very easily thermally excited and there appears a strong mixing of different spin states on the B sublattice.

Finally, it well known from general thermodynamic principles that the equilibrium Helmholtz free energy must be a concave function of temperature. The representative case confirming such a behavior is displayed in Fig. 5.21. Additionally, one can see from the figure that for negative values of d parameter, the temperature dependence of free energy starts from positive values.

Since at $T = 0$ the free energy equals to internal energy, then the boundary between $f > 0$ and $f < 0$ at $T = 0$ is given by $0 = -0.25J_4S_k^2 - dS_k^2$. At the ground state this causes, that the B sublattice of the system with spins S_k cannot take $\pm\frac{3}{2}$ values. This behavior shifts the system to significantly higher energy level. Subsequently, when the temperature increases, a number of decorating S_k spins flip to $\pm\frac{3}{2}$ states balancing the thermodynamic equilibrium. Here we can clearly see, how the higher value of negative crystal field pushes the system to the less favorable energy conditions.

6 Critical properties of the mixed spin-1/2 and spin-1 Ising model with three-site four-spin interaction on the honeycomb lattice

In previous sections we have discussed two models with three-site four-spin interaction on the square lattice, the bond of which have been decorated by spin-1 or by spin-3/2 atoms. The results presented for various physical quantities have revealed how the value of decorating spin influences magnetic properties of the system when others parameters are fixed. Another very interesting task related to the models under investigation is to clarify the influence of topology of underlying decorated lattice on its magnetic behavior. In order to put some insight on this problem, we will study in this section phase diagrams of the mixed spin-1/2 and spin-1 Ising model with three-site four-spin interaction on the honeycomb lattice.

6.1 Definition of the model and its exact solution

The system under investigation is represented by different kind of atoms with spins $\mu = 1/2$ and $S = 1$ arranged in a two-dimensional honeycomb lattice with the coordination number $z = 3$, as it is depicted in Fig. 6.1. That lattice may be apparently divided onto two interpenetrating sublattices with the equal number of lattice sites, to be denoted as A and B sublattice, respectively. The number of atoms on each separate sublattice will be by definition set to N, so that the total number of atoms on the whole honeycomb lattice will be $2N$.

The model presented in Fig. 6.1 can be readily solved exactly by applying the general formalism of $Y - \Delta$ transformation (see Subsec. 4.2). For this purpose, the total Hamiltonian is again expressed as a sum of site Hamiltonians, i.e.,

$$\mathcal{H} = \sum_{k=1}^{N} \mathcal{H}_k(S_k, \mu_{k1}, \mu_{k2}, \mu_{k3}), \tag{6.1}$$

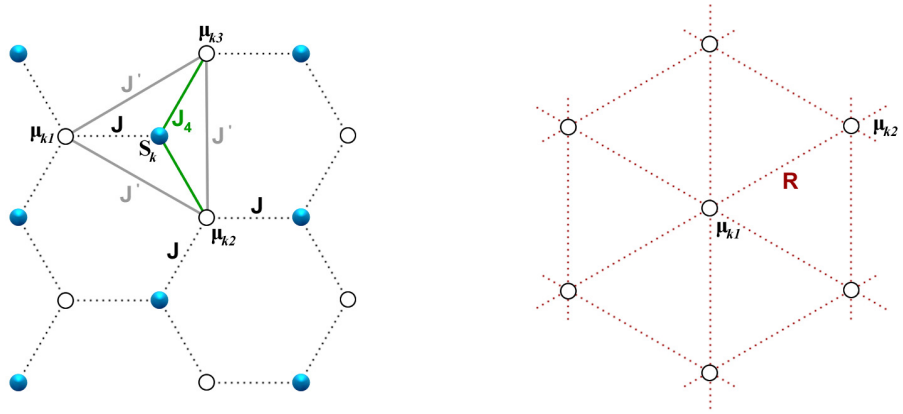

Fig. 6.1: Honeycomb lattice with the three-site four-spin interactions and corresponding simple triangular lattice that appears after its transformation.

where the site Hamiltonian $\mathcal{H}_k$ reads

$$\begin{aligned}\mathcal{H}_k = & - J(\mu_{k1}+\mu_{k2}+\mu_{k3})S_k - J'(\mu_{k1}\mu_{k2}+\mu_{k1}\mu_{k3}+\mu_{k2}\mu_{k3}) \\ & - J_4(\mu_{k1}\mu_{k2}+\mu_{k1}\mu_{k3}+\mu_{k2}\mu_{k3})S_k^2 - DS_k^2. \end{aligned} \tag{6.2}$$

Here the physical meaning of parameters J, J', J_4 and D is exactly the same as in Eq. (5.1). Now, following the standard procedures, one simply obtains the following relations for the partition function and the Helmholtz free energy of the system under investigation

$$\mathcal{Z}_h = A^N \mathcal{Z}_t(\beta R), \tag{6.3}$$

and

$$F_h = -Nk_BT\ln(A) + F_t(\beta R), \tag{6.4}$$

where the subscripts h and t denote the honeycomb and triangular lattice, respectively. The parameters A and R are in general given by (4.16) and for the functions V_1 and V_2 one simply derives from (4.17) and (4.18) the following expressions

$$V_1 = e^{\frac{3}{4}\beta J'}\left[1+2e^{\frac{3}{4}\beta J_4}e^{\beta D}\cosh\left(\frac{3}{2}\beta J\right)\right] \tag{6.5}$$

$$V_2 = e^{-\frac{1}{4}\beta J'}\left[1+2e^{-\frac{1}{4}\beta J_4}e^{\beta D}\cosh\left(\frac{1}{2}\beta J\right)\right]. \tag{6.6}$$

The Helmholtz free energy of the triangular spin-1/2 lattice $F_t = F_t(\beta R) = -k_BT\ln\mathcal{Z}_t(\beta R)$ has been obtained exactly [129–132] and it is given by

$$\begin{aligned} F_t = & - \frac{1}{8\pi^2\beta}\int_0^{2\pi}\int_0^{2\pi}\ln\left\{\left(1+D^2\right)^{3/2}+D^3-D[\cos\theta+\cos\phi+\cos(\theta+\phi)]\right\}d\theta d\phi \\ & - \frac{1}{\beta}\ln 2, \end{aligned} \tag{6.7}$$

where $D = \sinh(\beta R/2)$.

6.2 Ground state phase diagrams

We again start the ground state analysis by investigating the internal energy $U = \langle\mathcal{H}\rangle$ at $T = 0$. Similarly, as for the decorated square lattice, one obtains the internal energy in the form

$$\begin{aligned}\frac{U}{N} = & - J\left\langle(\mu_{k1}+\mu_{k2}+\mu_{k3})S_k\right\rangle - J'\left\langle\mu_{k1}\mu_{k2}+\mu_{k1}\mu_{k3}+\mu_{k2}\mu_{k3}\right\rangle \\ & - J_4\left\langle(\mu_{k1}\mu_{k2}+\mu_{k1}\mu_{k3}+\mu_{k2}\mu_{k3})S_k^2\right\rangle - D\left\langle S_k^2\right\rangle, \end{aligned} \tag{6.8}$$

where the values of correlations function on the r.h.s of previous equation can be simply deduced from the possible spin configuration at $T = 0$. The minimum values of the internal energy for a given spin configuration then determine which phase will be stable in the relevant sector of phase space. Similarly, as in the previous text, numerical results will be presented in terms of reduced dimensionless parameters $\alpha = J/J_4$, $\lambda = J'/J_4$ and $d = D/J_4$. The ground-state

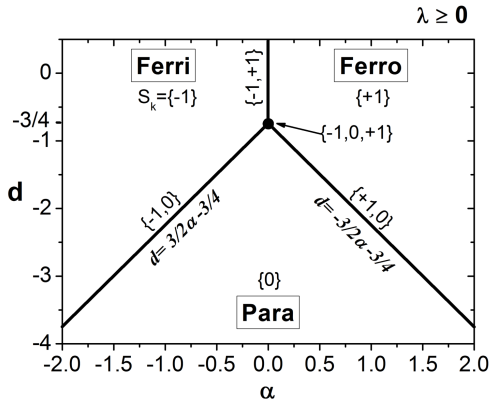

Fig. 6.2: Ground-state phase diagram for arbitrary non-negative values of λ. Displayed values in curly brackets denote values of spin S_k corresponding to each region. Values of spins μ_k are equal to $+\frac{1}{2}$ in the entire plane.

boundaries following from the above mentioned analysis are summarized in Fig. 6.2, where the phase diagram together with relevant spin configurations of decorating atoms are depicted.

The phases observed in relevant regions of Fig. 6.2 can be characterized as follows:
For $\lambda = 0$ and $\alpha = 0$ there are three different states:

- In the case of $d < -\frac{3}{4}$ the value $S_k = 0$ is preferred with paramagnetic ordering, phase III.
- In the case of $d = -\frac{3}{4}$ either of the values $S_k = \pm 1, 0$ are preferred at equal probability creating partially ordered phase VII.
- In the case of $d > -\frac{3}{4}$ the values $S_k = \pm 1$ are preferred at equal probability creating partially ordered phase VI.

For $\lambda = 0$ and $\alpha < 0$ there are the following states:

- In the case of $d < \frac{3}{2}\alpha - \frac{3}{4}$ the value $S_k = 0$ is preferred with paramagnetic ordering, phase III.
- In the case of $d = \frac{3}{2}\alpha - \frac{3}{4}$ the values $S_k = -1, 0$ are preferred at equal probability creating partially ordered phase IV.
- In the case of $d > \frac{3}{2}\alpha - \frac{3}{4}$ the value $S_k = -1$ is preferred with ferrimagnetic ordering, phase I.

For $\lambda = 0$ and $\alpha > 0$ there are also three different states:

- In the case of $d < -\frac{3}{2}\alpha - \frac{3}{4}$ the value $S_k = 0$ is preferred with paramagnetic ordering, phase III.

Phase	**Ordering**	**Entropy**	**Configuration**	
		$S/\left(\mathcal{N}k_B\right)$	μ_k	S_k
I.	ferrimagnetic	0	$+\frac{1}{2}$	-1
II.	ferromagnetic	0	$+\frac{1}{2}$	$+1$
III.	paramagnetic	0	$\pm\frac{1}{2}$	0
IV.	partially ordered	$\ln 2$	$+\frac{1}{2}$	$-1, 0$
V.	partially ordered	$\ln 2$	$+\frac{1}{2}$	$+1, 0$
VI.	partially ordered	$\ln 2$	$+\frac{1}{2}$	± 1
VII.	partially ordered	$\ln 3$	$+\frac{1}{2}$	$\pm 1, 0$

Tab. 6.1: Entropy and spin configurations in the ground state areas and also on their boundaries for $\lambda = 0$.

- In the case of $d = -\frac{3}{2}\alpha - \frac{3}{4}$ the values $S_k = +1, 0$ are preferred at equal probability creating partially ordered phase V.

- In the case of $d > -\frac{3}{2}\alpha - \frac{3}{4}$ the value $S_k = +1$ is preferred with ferromagnetic ordering, phase II.

The ground-state phase diagram of the present system is very similar as that one presented in Fig.5.2 for the decorated square lattice. The ferromagnetic, ferrimagnetic and paramagnetic phases are again stable in different regions of the phase space and they are separated by linear phase boundaries given by $d = \pm 3\alpha/2 - 3/4$. Of course, along these phase boundaries the relevant couples of phases may co-exist exhibiting a non-zero value of the entropy. Finally, as it is clear from our analysis, the partially ordered phases also exist for $\alpha = 0$, i.e., for the system with pure three-site four-spin interactions. Let us recall here that one should again treat all partially ordered phases as new separate phases of the system, to be consistent with the discussion in Subsec. 5.2 for the decorated square lattice.

It is also of interest to calculate the entropy of all ground-state phases. This task can be performed using the Boltzmann definition of entropy $S = \mathcal{N}k_B \ln \Omega$, where $\mathcal{N} = 2N$ determines the total number of lattice spins and Ω denotes the number of states. Obtained values of the entropy for every phase of the mixed spin-1/2 and spin-1 Ising model with three-site four-spin interaction on the honeycomb lattice are listed in Tab. 6.1.

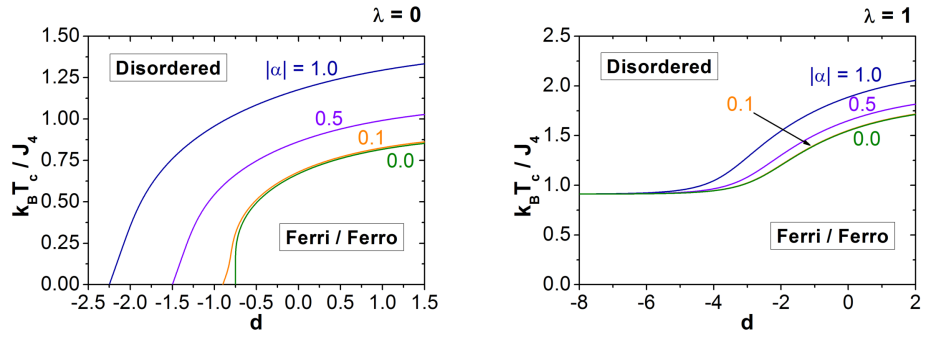

a) b)

Fig. 6.3: Phase diagrams in $d - T_c$ space for $\lambda = 0$ and 1.0.

6.3 Finite temperature phases and phase transitions

In order to derive an equation for finite-temperature phase diagrams one substitutes the value of inverse critical temperatureof the spin-1/2 triangular lattice (i.e., $\beta_{ct}R = \ln 3$) into Eq. (4.16) and then using Eqs. (6.5) and (6.5) we easily obtains the following relation

$$\lambda\beta_c J_4 + \ln\left[\frac{1}{3}\frac{1+2e^{\frac{3}{4}\beta_c J_4}e^{d\beta_c J_4}\cosh\left(\frac{3}{2}\alpha\beta_c J_4\right)}{1+2e^{-\frac{1}{4}\beta_c J_4}e^{d\beta_c J_4}\cosh\left(\frac{1}{2}\alpha\beta_c J_4\right)}\right] = 0. \tag{6.9}$$

The phase diagrams in $d - T_c$ space for $\lambda = 0$ and $\lambda = 1.0$ obtained from Eq. (6.9) are depicted In Figs. 6.3a) and b). As one can see, the the presented results are very similar as those in Figs.(5.3)a) and b) for the decorated square lattice. The main difference is that for the present model are all phase boundaries shifted to higher temperature region, so that magnetic ordering (including the partial ordering) now exists in a wider region of the phase space. Moreover, for the mixed-spin honeycomb lattice one does not observe the re-entrant behavior. These differences, as compared to decorated square lattice, may be attributed to geometric structure of the honeycomb and also to the structure of triangular lattice. Next, an alternative view on the phase diagrams in the $\alpha - T_c$ space for $\lambda = 0$ and $\lambda = 1.0$ is shown in Figs. 6.4a) and b). The results exhibit an expected symmetry around the line $\alpha = 0.0$ and they are in a full agreement with the ground-state phase diagram, shown in Fig. 6.2.

In order to illustrate the fundamental influence of the of the non-zero interaction J' on the phase boundaries, there are in Figs. 6.5a) and b) compared critical surfaces of the mixed spin-1/2 and spin-1 honeycomb lattice lattice for $\lambda = 0.0$ and $\lambda = 1.0$, respectively. Here we again observe qualitatively very similar results as those in the case of the mixed spin-1/2 and spin-1 decorated square lattice. One can clearly see that non-zero λ (i.e., $J' \neq 0$) shifts the critical surface towards high temperatures, so that no intersection of this surface with the $\alpha - d$ plane can appear. Consequently, the ground state will be always at least partially ordered.

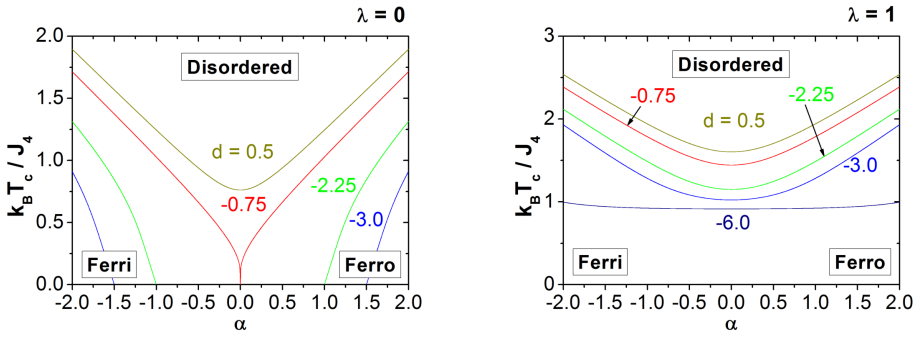

a) b)

Fig. 6.4: Phase diagrams in $\alpha - T_c$ space for $\lambda = 0$ and 1.0.

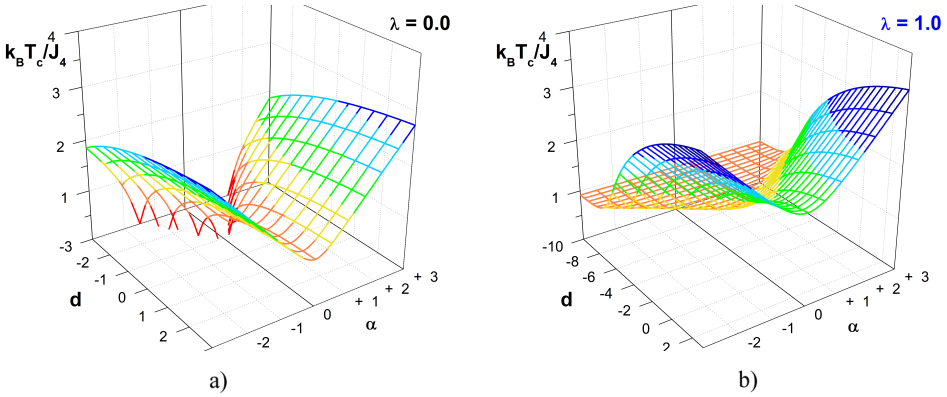

a) b)

Fig. 6.5: Phase diagram in $d - \alpha - T_c$ space for $\lambda = 0.0$ a) and for $\lambda = 1$ b).

Finally, it is worth emphasizing that all other physical quantities of the present model will exhibit qualitatively similar behavior as those of the mixed spin-1/2 and spin-1 decorated square lattice, therefore we will not analyze them in this work.

7 Magnetic and critical properties of the decorated triangular lattice with spin 1/2 and 3/2 and three-site four-spin interactions

The main attention is in this part focused on additional clarifying of the influence of multispin interactions on magnetic properties of a decorated triangular system. For this purpose we will again study the mixed spin-1/2 and spin-3/2 Ising model with three-site four-spin interactions (see Fig. 7.1). The ground state, phase diagrams, entropy and magnetization will be discussed and compared with the results obtained for similar models in previous sections. It is clear that such a triangular model is in many regards very similar to that one studied on the decorated square lattice in Subsec. 5.3. Consequently, we can use here all relations derived before with only few small modifications. For this reason, one can now formulate the theory in a very compact form, emphasizing mainly the differences arising due to different geometrical structure of the decorated triangular lattice.

The total Hamiltonian of the system is again defined as a sum of bond Hamiltonian, i.e.,

$$\mathcal{H} = \sum_{k}^{3N} \mathcal{H}_k, \tag{7.1}$$

where the bond Hamiltonian $\mathcal{H}_k$ has the usual form

$$\mathcal{H}_k = -J(\mu_{k1} + \mu_{k2})S_k - J'\mu_{k1}\mu_{k2} - J_4\mu_{k1}\mu_{k2}S_k^2 - DS_k^2. \tag{7.2}$$

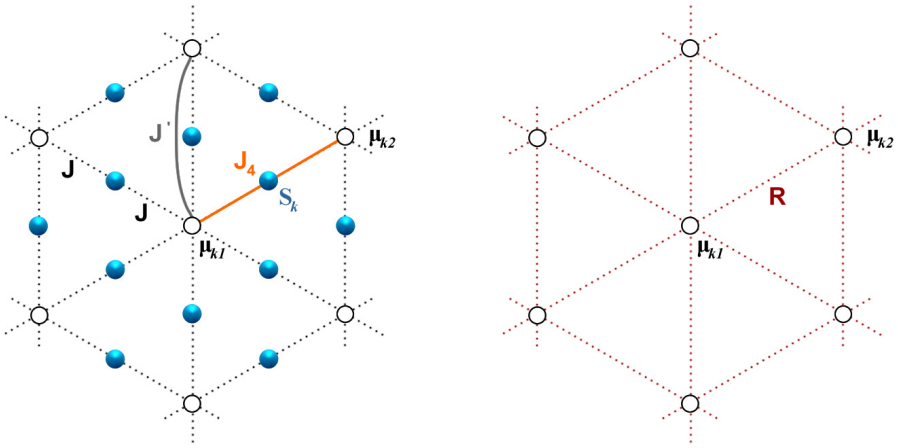

Fig. 7.1: Fragments of the triangular lattices. Left: Decorated triangular lattice under investigation, where doted lines denote bilinear interactions J, black lines denote bilinear interactions J' and orange lines indicate three-site four-spin interactions J_4. The open circles display μ_{ki} atoms creating a sublattice A and full, light-blue colored ones display decorating S_k atoms creating a sublattice B. Right: Original triangular lattice with a simple nearest neighbors bilinear interaction R and μ_{ki} atoms.

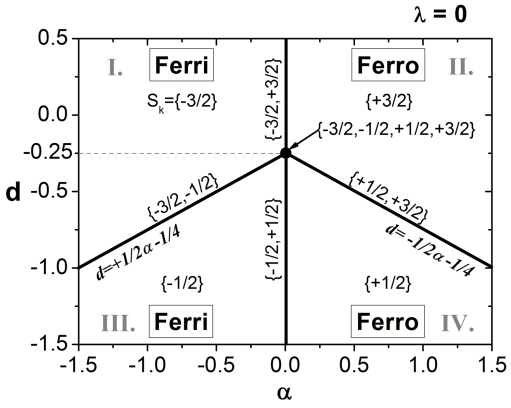

Fig. 7.2: Ground-state phase diagram with S_k spin values matching each phase.

The meaning of all parameters in previous equation is the same as in Eq. (5.1) and spin variables take the values $\mu_{ki} = \pm 1/2$ and $S_k = \pm 1/2, \pm 3/2$, as it follows from the definition of the model (see Fig. 7.1). Taking into account previous relations, one easily applies the general formalism developed in Sec. 4 to the present model and obtains for the partitions functions the following expression

$$\mathcal{Z} = A^{3N} \mathcal{Z}_t(\beta R). \tag{7.3}$$

In the previous equation $\mathcal{Z}_t(\beta R)$ represents the partition function of the spin-1/2 Ising model on the triangular lattice which of course known exactly [129–132]. The parameters A and R are given by Eqs (5.3), (5.6)-(5.9), and the Helmholtz free energy takes the form

$$F(\beta, J, J_4, J', D) \quad = \quad -3N\beta^{-1} \ln A(\beta, J, J_4, J', D) + F_t(\beta R), \tag{7.4}$$

where the Helmholtz free energy energy of the non-decorated spin-1/2 triangular lattice $F_t(\beta R)$ is given by (6.7).

7.1 Ground-state phase diagram

Similarly as in previous cases, one has at first to analyze the internal energy of the system, which is given by

$$\frac{U}{3N} = -J\big\langle(\mu_{k1}^z + \mu_{k2}^z)S_k^z\big\rangle - J'\big\langle\mu_{k1}^z\mu_{k2}^z\big\rangle - J_4\big\langle\mu_{k1}^z(S_k^z)^2\mu_{k2}^z\big\rangle - D\big\langle(S_k^z)^2\big\rangle. \tag{7.5}$$

Substituting all possible spin configurations into previous equation and looking for its global minima, one obtains the ground-state phase diagram as it is depicted in reduced variables in Fig. 7.2 for $\lambda = 0.0$. In the figure, there are also shown possible spin configurations in relevant phases. As one can see, the ground-state phase diagram of the decorated triangular system is

identical with that one of the mixed spin-1/2 and spin-3/2 Ising model on the decorated square lattice. This is obviously a consequence of the fact that the internal energies reduced per one bond are given by the same formula for both decorated lattices (see Eqs. (5.42) and (7.5)). Moreover, it easy to understand that other decorated lattices will have also the same reduced internal energy. Thus one can conclude that ground state of all models with spin-3/2 decorating atoms will have the same ground-state phase diagram independently of the lattice structure, assuming that they are described by the same bond Hamiltonian (7.2).

Indeed, for the present model one again finds four different ordered phases that are separated by phase boundaries at which the system undergoes the first order phase transitions. Along relevant phase boundaries takes place the mixing of neighboring phases, so that one again observes there partially ordered phases with non-zero entropy at $T = 0.0$.

The careful analysis of the phase boundaries leads to following conclusions:

- In the case of $\alpha = 0$, $d = -\frac{1}{4}$ either of the value $S_k = \pm\frac{3}{2}, \pm\frac{1}{2}$ is preferred with equal probability.
- In the case of $\alpha = 0$, $d > -\frac{1}{4}$ the values $S_k = \pm\frac{3}{2}$ are preferred.
- In the case of $\alpha = 0$, $d < -\frac{1}{4}$ the values $S_k = \pm\frac{1}{2}$ are preferred.
- In the case of $\alpha < 0$, $d = \frac{1}{2}\alpha - \frac{1}{4}$ either of the value $S_k = -\frac{3}{2}, -\frac{1}{2}$ is preferred with equal probability.
- In the case of $\alpha > 0$, $d = -\frac{1}{2}\alpha - \frac{1}{4}$ either of the value $S_k = +\frac{3}{2}, +\frac{1}{2}$ is preferred with equal probability.

On basis of this analysis one easily calculates possible values of the entropy at $T = 0$ that are summarized in Table 7.1.

Moreover, one easily finds, that switching on the pair exchange interaction J' will not change the ground-state phase diagram.

7.2 Finite temperature properties

Although we have found for the decorated triangular system the same ground-state phase diagram as in that one for the decorated square lattice, one can see from Eqs.(5.42) and (7.5) that the value of the total internal energy of the triangular decorated lattice is at $T = 0$ lower than the total internal energy of the decorated square lattice. It is therefore of interest to investigate how this difference in total internal energies will influence the phase diagrams at finite temperatures.

The equation for critical boundaries of the mixed spin-1/2 and spin-3/2 sing model on decorated triangular lattice can easily found utilizing Eqs. (5.6)-(5.9) and takes the following form

$$\ln 3 = \beta_c \left(J' + \frac{9}{4} J_4 \right) + 2 \ln \frac{\cosh\left(\frac{3}{2}\beta_c J\right) + \mathrm{e}^{-2\beta_c (D + \frac{J_4}{4})} \cosh\left(\frac{1}{2}\beta_c J\right)}{1 + 2\mathrm{e}^{-2\beta_c (D - \frac{J_4}{4})}}, \tag{7.6}$$

with $\beta_c = 1/(k_B T_c)$. In deriving of Eq. (7.6) one applies the fact that the inverse critical temperature of the spin-1/2 triangular lattice is given by $\beta_c R = \ln 3$.

Phase	**Ordering**	**Entropy**	**Configuration**	
		$S/\left(Nk_B\right)$	μ_k	S_k
I.	ferrimagnetic	0	$+\frac{1}{2}$	$-\frac{3}{2}$
II.	ferromagnetic	0	$+\frac{1}{2}$	$+\frac{3}{2}$
III.	ferrimagnetic	0	$+\frac{1}{2}$	$-\frac{1}{2}$
IV.	ferromagnetic	0	$+\frac{1}{2}$	$+\frac{1}{2}$
I./II.	partially ordered	$\ln 2^2$	$+\frac{1}{2}$	$-\frac{3}{2},+\frac{3}{2}$
I./III.	partially ordered	$\ln 2^2$	$+\frac{1}{2}$	$-\frac{3}{2},-\frac{1}{2}$
II./IV.	partially ordered	$\ln 2^2$	$+\frac{1}{2}$	$+\frac{1}{2},+\frac{3}{2}$
III./IV.	partially ordered	$\ln 2^2$	$+\frac{1}{2}$	$-\frac{1}{2},+\frac{1}{2}$
I./II./III./IV.	partially ordered	$\ln 2^4$	$+\frac{1}{2}$	$-\frac{3}{2},-\frac{1}{2},+\frac{1}{2},+\frac{3}{2}$

Tab. 7.1: Entropy and spin configurations in the ground state areas and also on their boundaries for $\lambda = 0$.

Solving previous equation numerically, one obtains phase diagrams that are in a perfect agreement with the ground-state phase diagram (see Fig. 7.2). As expected, the phase diagrams for the decorated triangular lattice presented in Figs. 7.3 and 7.4 are very similar to corresponding results for the decorated square lattice (see Figs. 5.11 and 5.13). The main difference is that all phase boundaries are now shifted towards higher temperature region and this effect can be clearly attributed to the higher co-ordination number of the original triangular lattice ($z = 6$). Next, comparing the results for $\lambda = 0.0$ and $\lambda = 1.0$ one can conclude that the next-nearest neighbor bi-linear exchange J' causes increase of the critical temperature T_c and thus enhancing of ordered region, as one can see comparing Figs. 7.3b)-7.3b) with Figs. 7.4a)- 7.5b), respectively. Finally, the critical surfaces depicted in Figs. 7.5 clearly illustrate that the paramagnetic phase can never be stable at $T = 0.0$, since the critical surfaces do not intersect the $d - \alpha$ plane. In addition, comparing the results for the lattices decorated with spin-3/2 atoms with those obtained for decorating spin-1 atoms, one can conclude that the paramagnetic phase can be stable at $T = 0$ only if decorating atoms have an even spin.

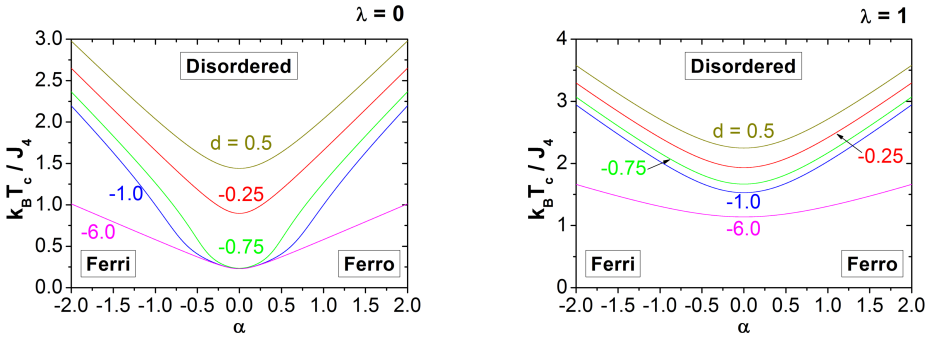

a) b)

Fig. 7.3: Phase diagrams in $\alpha - T$ space a) for $\lambda = 0$, b) for $\lambda = 1$.

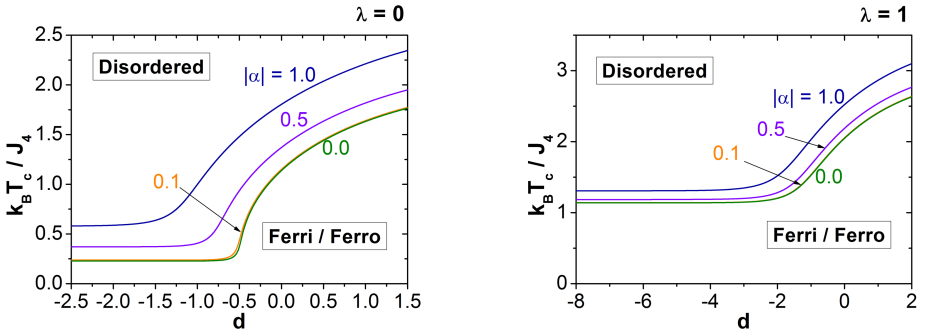

a) b)

Fig. 7.4: Phase diagrams in $d - T$ space a) at $\lambda = 0$, b) at $\lambda = 1$.

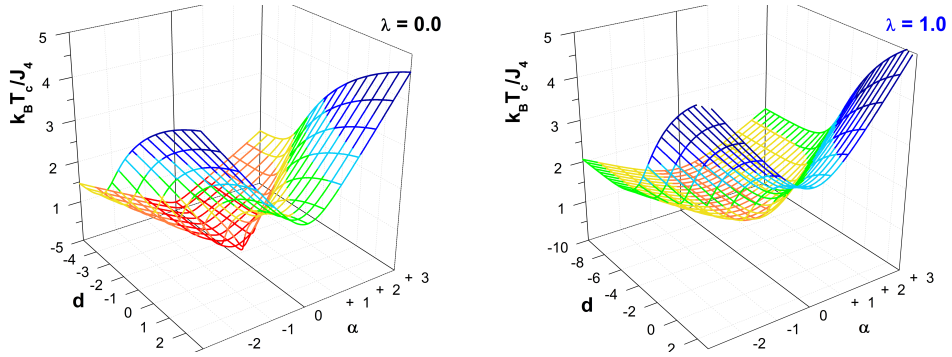

a) b)

Fig. 7.5: Phase diagrams in $d - \alpha - T$ space a) for $\lambda = 0$, b) for $\lambda = 1$.

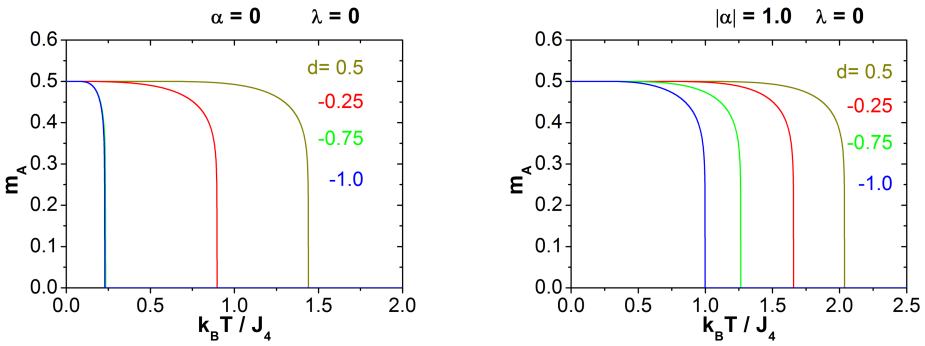

a) b)

Fig. 7.6: Magnetization per 1 spin on the sublattice A dependence on k_BT/J_4 for $\lambda = 0$ and a) at $\alpha = 0$, b) at $|\alpha| = 1$ and several typical values of d.

7.3 Magnetization

The analysis presented in previous section can be significantly supported by calculating thermal variations of the sublattice and total reduced magnetizations.

The total magnetization of the decorated triangular lattice reduced per one atom is given by

$$m = \frac{1}{4}\left(m_A + 3m_B\right), \tag{7.7}$$

where the reduced sublattice magnetizations m_A and m_B are defined as

$$m_A = \langle \mu_{ki} \rangle \tag{7.8}$$

and

$$m_B = \langle S_k \rangle . \tag{7.9}$$

Applying general equations (5.31) one simply gets

$$m = \frac{1}{4}(1 + 3A_1)m_t, \tag{7.10}$$

where the coefficient A_1 is given by (5.26).

The magnetization $m_t\left(\beta R\right) = \langle \mu_{ki} \rangle_t$ of the original non-decorated triangular lattice has been already analytically calculated by Potts [133] in the form

$$m_t = \langle \mu_k \rangle_0 = \frac{1}{2}\left(1 - \frac{16a^6}{\left(1+3a^2\right)\left(1-a^2\right)^3}\right)^{\frac{1}{8}}, \; a = \mathrm{e}^{-\frac{\beta R}{2}}. \tag{7.11}$$

The numerical results obtained for sublattice magnetizations using previous formulas are for $\lambda = 0.0$, $\alpha = 0$ and $|\alpha| = 1.0$ shown in Figs. 7.6a) and 7.6b) . The most important

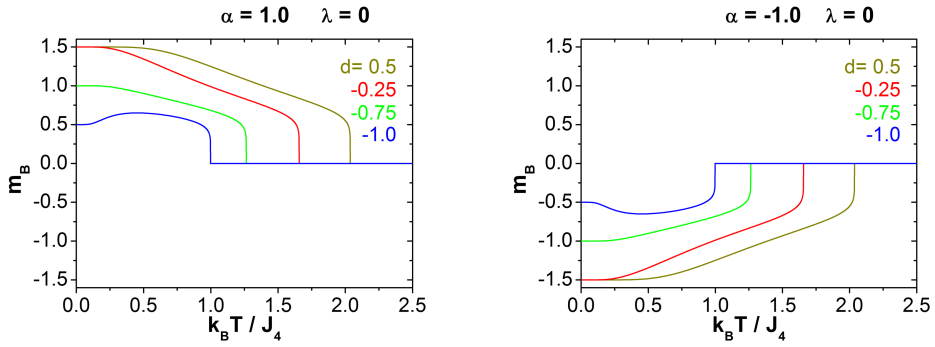

a) b)

Fig. 7.7: Magnetization per 1 spin on the sublattice B dependence on k_BT/J_4 in several significant d values for $\lambda = 0$ and a) at $\alpha = +1$, b) at $\alpha = -1$.

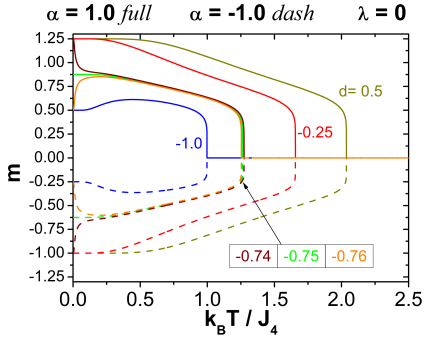

Fig. 7.8: Total magnetization per 1 spin dependence on k_BT/J_4 in several significant d values for $\alpha = \pm 1$ and $\lambda = 0$.

finding following from the figures is that the sublattice magnetization m_A takes its saturated value $m_A = 0.5$ at $T = 0.0$ for an arbitrary set of interaction parameters. On the other hand, the saturated value of m_B strongly depends on the value of α and in agreement with the ground-state analysis one finds the following three possibilities:

- $m_B = 0$ for $\alpha = 0$
- $m_B > 0$ for $\alpha > 0$
- $m_B < 0$ for $\alpha < 0$

The thermal variations of m_B are for $\alpha \pm 1$ depicted in Figs. 7.7. Finally, the total magnetization as a function of temperature may be seen in Fig. 7.8 for $\alpha \pm 1$. Accordingly, there are six different magnetization levels at $T = 0$ depending on the value of d.

8 Magneto-elastic and spin-phonon interaction on triangular lattice

In this part we will briefly comment on magnetic properties of a spin system on the triangular lattice where beside conventional spin-spin interactions are present also magneto-elastic and spin-phonon interactions.

8.1 Definition of the model and its exact solution

The system under investigation is a mixed spin-1 and spin-1/2 Ising model on the two-dimensional triangular lattice with several different interactions as it is shown in Fig. 8.1 a).

The vertices of each triangle are occupied by A-type atoms with spin variable μ_{ki} assumed to take the values $\mu_{ki} = \pm\frac{1}{2}$, while in the middle of each edge are located B-type atoms with spin variable S_k assumed to take the values $S_k = \pm 1, 0$. The total number of A-type atoms is N and the total number of bonds is $Nz/2 = 3N$, where z denotes coordination number of the non-decorated lattice. The total number of B-type atoms is equal to the total number of bonds, so it equals $3N$. From now on, we simply name A-type atoms as μ_{ki} spins and B-type atoms as S_k spins and therewith the word bond means one entire edge of the triangle created by two A-type atoms. In contrast to previously investigated models, the S_k spins are allowed to vibrate harmonically around a mean position located in the middle of the relevant bond.

Due to magneto-elastic properties, the magnetic energy of the k-th bond must be mathemati-

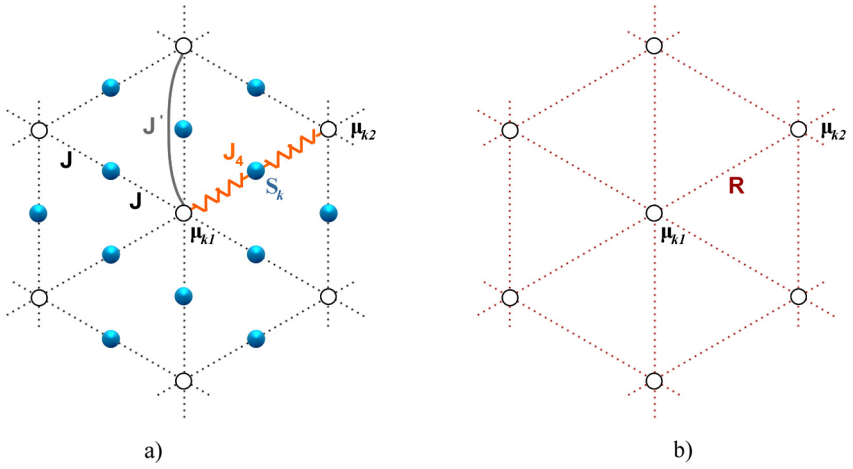

Fig. 8.1: a) The fragment of the decorated triangular lattice under investigation. The doted lines denote bilinear interactions J between nearest neighbors and orange lines indicate three-site four-spin interactions J_4. The open circles display spin-1/2 atoms creating a sublattice A and full, light-blue colored ones, display decorating spin-1 atoms positioned flexibly and creating a sub-lattice B. b) The fragment of the original undecorated triangular lattice occupied with μ_{ki} spins which are coupled with R interaction.

cally described by the modified bond Hamiltonian which takes the form

$$\hat{\mathcal{H}}_k^{(me)} = -DS_k^2 - JS_k\left[\left(1-\varepsilon\hat{x}_k\right)\mu_{k1} + \left(1+\varepsilon\hat{x}_k\right)\mu_{k2}\right]. \tag{8.1}$$

Here J denotes the bilinear exchange interaction between nearest neighbors $\mu_{ki} - S_k$, D indicates a single-ion anisotropy parameter and $\hat{x}_k$ stands for the position operator of S_k spin. The interaction parameters J, D are allowed to take arbitrary positive or negative values. The elasticity of the $k-th$ bond is expressed by means of the parameter ε representing the impact of change of S_k spin position to the magnitude of J interaction.

The energy of quantum harmonic oscillations of decorating B-type atoms with spin variable S_k can be obviously described using the phononic part of Hamiltonian, i.e.,

$$\hat{\mathcal{H}}_k^{(ph)} = \frac{1}{2}\frac{\hat{p}_k^2}{m} + \frac{1}{2}K_2\left(-\hat{x}_k\right)^2 + \frac{1}{2}K_2\left(+\hat{x}_k\right)^2, \tag{8.2}$$

where $\hat{p}_k$ is the momentum operator of B-type atoms and K_2 means the stiffness constant of $\mu_k - S_k$ bond (a greater value for K_2 signifies a tighter bond).

The total Hamiltonian of the system is then given by

$$\hat{\mathcal{H}} = \sum_{k=1}^{3N}\left(\hat{\mathcal{H}}_k^{(me)} + \hat{\mathcal{H}}_k^{(ph)}\right) \tag{8.3}$$

and contributions to the bond Hamiltonians can be, respectively, rewritten as

$$\hat{\mathcal{H}}_k^{(me)} = -DS_k^2 - JS_k\left(\mu_{k1}+\mu_{k2}\right) - L\hat{x}_kS_k\left(-\mu_{k1}+\mu_{k2}\right) \tag{8.4}$$

$$\hat{\mathcal{H}}_k^{(ph)} = \frac{1}{2}\frac{\hat{p}_k^2}{m} + K_2\hat{x}_k^2, \tag{8.5}$$

where the new parameter $L = J\varepsilon$ in (8.4) can be interpreted as an effective two-spin interaction appearing due to small change of S_k spin position.

In order to determine the partition function one firstly needs to separate the magnetic variables from the position operators in (8.4). For this purpose we introduce the following canonical transformations [134], [135]

$$\hat{x}_k = \hat{X}_k + \frac{1}{2}\frac{L}{K_2}S_k\left(-\mu_{k1}+\mu_{k2}\right), \tag{8.6}$$

and

$$\hat{p}_k = \hat{P}_k. \tag{8.7}$$

Substituting previous equations into (8.4) and (8.5) one obtains

$$\mathcal{H}_k^{(M)} = -JS_k\left(\mu_{k1}+\mu_{k2}\right) - DS_k^2 - \frac{1}{8}\frac{L^2}{K_2}S_k^2 + \frac{1}{2}\frac{L^2}{K_2}S_k^2\mu_{k1}\mu_{k2} \tag{8.8}$$

$$\hat{\mathcal{H}}_k^{(P)} = \frac{1}{2}\frac{\hat{P}_k^2}{m} + K_2\hat{X}_k^2. \tag{8.9}$$

As one can see the transformation procedure introduced above really separates magnetic and translation degrees of freedom and mathematically generates a new effective multispin interaction which is surprisingly the well-known three-site four-spin interaction. Consequently, the total bond Hamiltonian takes the form

$$\hat{\mathcal{H}}_k = \mathcal{H}_k^{(M)} + \hat{\mathcal{H}}_k^{(P)} \tag{8.10}$$

and the total partition function of the present system can be expressed as

$$\mathcal{Z} = \sum_{\{\mu_{ki}\}} \prod_{k=1}^{3N} \mathcal{Z}_k^{(M)} \mathcal{Z}_k^{(P)} \tag{8.11}$$

or

$$\mathcal{Z} = \left(\mathcal{Z}_k^{(P)}\right)^{3N} \sum_{\{\mu_{ki}\}} \prod_{k=1}^{3N} \mathcal{Z}_k^{(M)}, \tag{8.12}$$

where

$$\mathcal{Z}_k^{(P)} = \sum_{n=0}^{\infty} \mathrm{e}^{-\beta\hbar\omega\left(n+\frac{1}{2}\right)}, \quad \omega^2 = \frac{2K_2}{m} \tag{8.13}$$

and

$$\mathcal{Z}_k^{(M)} = \sum_{S_k=0,\pm1} \mathrm{e}^{-\beta\mathcal{H}_k^{(M)}}. \tag{8.14}$$

After evaluating the summation in (8.13) and (8.14), one obtains for the phononic and magnetic partition function of k-th bond the following simple expressions

$$\mathcal{Z}_k^{(P)} = \frac{1}{2\sinh\left(\frac{1}{2}\beta\hbar\omega\right)}. \tag{8.15}$$

and

$$\mathcal{Z}_k^{(M)} = 2e^{\beta D} e^{\frac{1}{8}\beta\frac{L^2}{K_2}} e^{-\frac{1}{2}\beta\frac{L^2}{K_2}\mu_{k1}\mu_{k2}} \cosh\left[\beta J\left(\mu_{k1}+\mu_{k2}\right)\right] + 1. \tag{8.16}$$

Using Eq. (8.15) and introducing the total partition function of magnetic subsystem

$$\mathcal{Z}^{(M)} = \sum_{\{\mu_{ki}\}} \prod_{k=1}^{3N} \mathcal{Z}_k^{(M)}, \tag{8.17}$$

one rewrites Eq.(8.12) as

$$\mathcal{Z} = \left(\frac{1}{2\sinh\left(\frac{1}{2}\beta\hbar\omega\right)}\right)^{3N} \mathcal{Z}^{(M)}, \tag{8.18}$$

and moreover, one may evaluate the magnetic partition function $\mathcal{Z}^{(M)}$ applying the decoration-iteration transformation (see Sec.5). After a straightforward calculation one obtains

$$\mathcal{Z}^{(M)}\left(\beta, J, L, K, D\right) = A^{3N}\mathcal{Z}_t\left(\beta R\right), \tag{8.19}$$

where $\mathcal{Z}_t\left(\beta R\right)$ is of course the partition function of the spin-1/2 triangular lattice [129–132] and R represents the interaction present in that original triangular lattice as it is depicted in Fig. 8.1 b). The equations for transformation parameters A and βR take the standard form, i.e.

$$\beta R = 2\ln\frac{w_1}{w_2} \tag{8.20}$$

and

$$A^2 = w_1 w_2, \tag{8.21}$$

where

$$w_1 = 2\mathrm{e}^{\beta D}\cosh\left(\beta J\right) + 1 \tag{8.22}$$

$$w_2 = 2\mathrm{e}^{\beta D}\mathrm{e}^{\frac{1}{4}\beta\frac{L^2}{K_2}} + 1. \tag{8.23}$$

Obviously, the total magnetization per one site of decorated lattice comprises both sublattice magnetization in the following way

$$m = \frac{1}{4}\left(m_A + 3m_B\right), \tag{8.24}$$

where for the evaluation of m_A and m_B one may apply all procedures and equations derived in Sec. 5

8.2 Ground state phase diagram

We will now briefly review numerical results for the model under investigation using the reduced dimensionless parameters $d = D/J$, $\kappa_2 = K_2/J$ and $\varepsilon = L/J$. In order to establish the ground state of the system, we has to find global minima of the total reduced internal energy, which now takes the form

$$\frac{U}{3NJ} = -\left\langle S_k\left(\mu_{k1} + \mu_{k2}\right)\right\rangle - d\left\langle S_k^2\right\rangle - \frac{1}{8}\frac{\varepsilon^2}{\kappa_2}\left\langle S_k^2\right\rangle - \frac{1}{2}\frac{\varepsilon^2}{\kappa_2}\left\langle S_k^2\mu_{k1}\mu_{k2}\right\rangle + \frac{\hbar\omega}{J}. \tag{8.25}$$

In general, the existence ans stability of various phases in the decorated system depend also on the behavior of the original lattice, therefore it is very useful to investigate also the parameter βR in the limit of $\beta \to \infty$, i.e.,

$$\lim_{\beta\to\infty}\beta R = \lim_{\beta\to\infty} 2\ln\frac{2\cosh(\beta J) + \exp(-d\beta J)}{2\exp\left(\dfrac{\varepsilon^2}{4\kappa_2}\beta J\right) + \exp(-d\beta J)}. \tag{8.26}$$

On the basis of this analysis one can discern five different regimes of βR interaction that are listed in Tab. 8.1. As one can see, the competition of single-ion anisotropy term $\exp(-d\beta J)$

βR **interaction value**	**Region**	$\langle \mu_k \rangle$	$\langle S_k \rangle$
$\beta R \to \infty$	Ferromagnetic	$\frac{1}{2}$	1
$0 < \beta R \approx 1.39 < \infty$	Ferro-Paramagnetic	0.475	0.475
$\beta R = 0$	Paramagnetic	0	0
$\infty < \beta R \approx -0.81 < 0$	Ferro-Antiferro, Paramagnetic		
$\beta R \to -\infty$	AntiFerromagnetic		

Tab. 8.1: Table of spin mean values for various βR interaction values at zero-temperature limit for $\lambda = 0$ and $\kappa_2 = 1$. In this βR analysis, $\langle \mu_k \rangle$ and $\langle S_k \rangle$ values for AF states are not calculated because here used formula for $\langle \mu_k \rangle$ is valid for the ferromagnetic phase only.

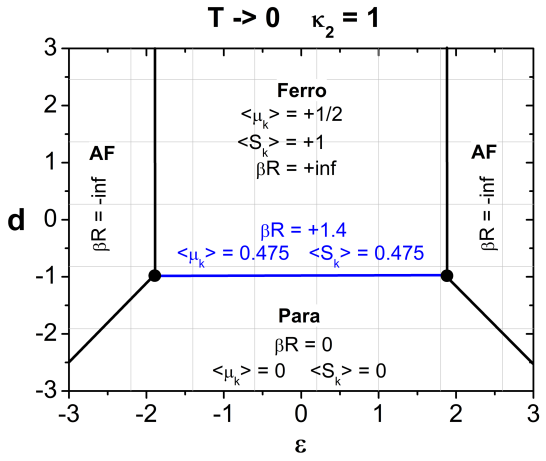

Fig. 8.2: Ground-state phase diagram in $\varepsilon - d$ space for $\kappa = 1.0$. Ferro denotes ferromagnetic state, Para means paramagnetic state and AF indicates anti-ferromagnetic state.

at the point $d = -1$ with the nearest neighbor bilinear interaction term $\cosh(\beta J)$ is just the reason causing the finite and also non-zero βR limit here. Thus, the competition of single-ion anisotropy term with another interaction is the reason inflicting the special partially ordered phase with non-saturated magnetic order $m_A = m_B = 0.475$ at zero temperature. The typical ground-state diagram in $\varepsilon - d$ plane is depicted in Fig. 8.2 for $\kappa = 1.0$ and similarly as in other works [135], the range of ε is left to be large enough in order to identify all possible phases in the system. One can see from the figure that three standard magnetic phases (ferromagnetic,

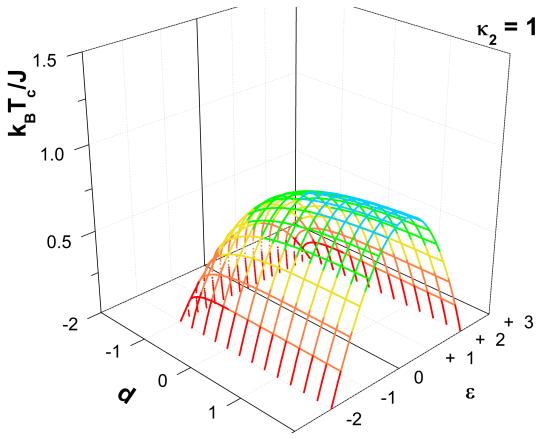

Fig. 8.3: The dependence of critical temperature on the single-ion anisotropy d and bond elasticity ε.

antiferromagnetic and paramagnetic) may exist in different regions of the phase space. Along phase boundaries the relevant couples of phases may co-exist, thus the system will exhibit a first order phase transition when crossing a phase boundary. Additionally, for $d = -1$, one observes again an unusual partially ordered phase with $m_A = m_B = 0.475$. Although this value exactly coincides with the value of m_A obtained for the partially ordered phase in the mixed spin-1/2 and spin-1 Ising model on decorated square lattice (see Subsec. 5.2), there is a principal difference between two cases. Namely, the above mentioned partially ordered phase appears on the decorated square lattice only if all pair exchange interactions are zero and moreover one also finds there the sublattice magnetization $m_B = 0.0$. In the present system, the pair interaction is non-zero and the partially disordered phase has also $m_B = 0.475$. Another important finding is that such a partially ordered phase apparently appears also in the system with $\varepsilon = 0.0$, which corresponds to the standard mixed spin-1/2 and spin-1 decorated triangular lattice. In fact, this findings are very surprising and indicate that in the investigation of standard decorated lattices has been overlooked the existence of very interesting unconventional magnetic phase.

8.3 Finite temperature phase diagrams and magnetization

The finite temperature phase transitions can be obtained solving the following equation numerically

$$\ln 3 = 2 \ln \frac{2\cosh(\beta_c J) + \exp(-d\beta_c J)}{2\exp\left(\dfrac{\varepsilon^2}{4\kappa_2}\beta_c J\right) + \exp(-d\beta_c J)}. \tag{8.27}$$

At first, in Fig. 8.3 there is depicted a global view on the critical surface taking parameters d and ε as independent variables. As one can see, the critical surface enwraps the region of ferromagnetically ordered states, where both sub-lattice magnetizations have nonzero values and

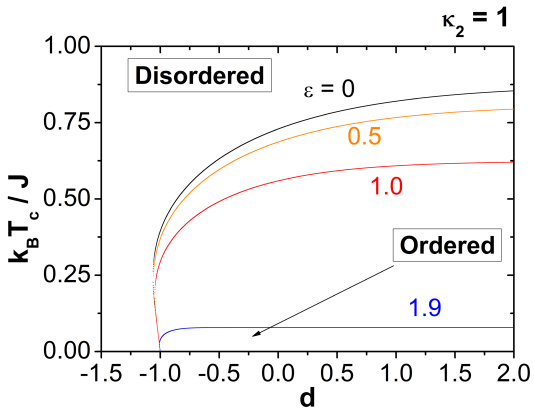

Fig. 8.4: Phase diagram in $d - T$ space for the system with nearest neighbor spin interaction.

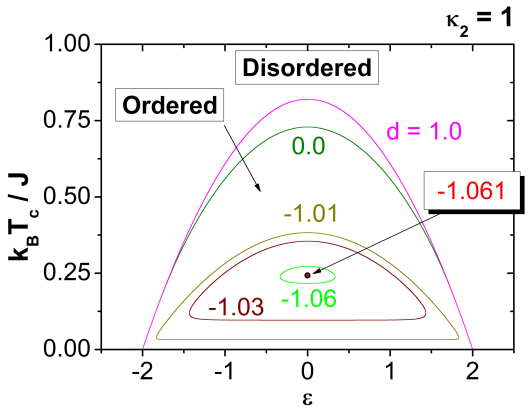

Fig. 8.5: Phase diagram in $\varepsilon - T$ space for the system with $\kappa = 1.0$.

one should also note that these ordered states are firmly restricted to particular values of elasticity and single-ion anisotropy parameters, namely $d > -1$ and $|\varepsilon| < 2$. In order to uncover further details, that are to a large extent lost in three-dimensional picture, we present in Figs. 8.4 and 8.5 two dimensional variations of critical temperature. The dependence of critical temperature on single-ion anisotropy d is illustrated in Fig. 8.4 for several typical values of elasticity. As usually, above each critical line, the system $d > -1$ support the existence of ordered state bellow a proper critical temperature. On the other hand, the increasing elasticity destroys the magnetic ordering and supports the paramagnetic phase at lower temperatures and as it follows from Fig. 8.5 for values $|\varepsilon| \geq 2$ the elasticity prevents to get ordered state at any temperature.

Next one should notice the critical curves in Fig. 8.5 corresponding to specific single-ion

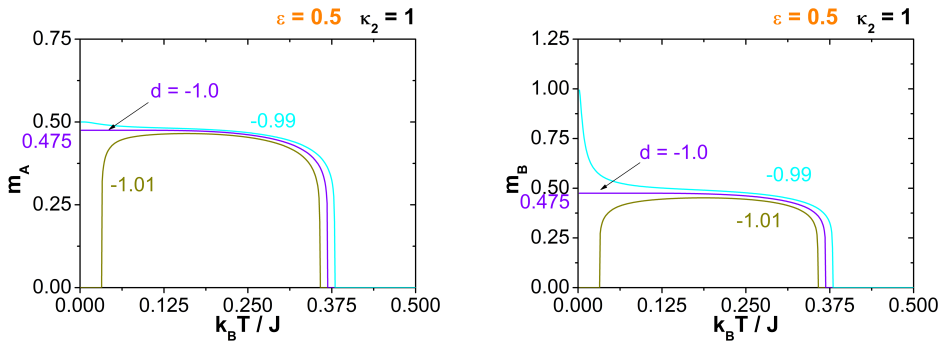

Fig. 8.6: The temperature dependence of sublattice magnetizations m_A and m_B for $\varepsilon = 0.5$ and $\kappa_2 = 1$ and three representative values of d

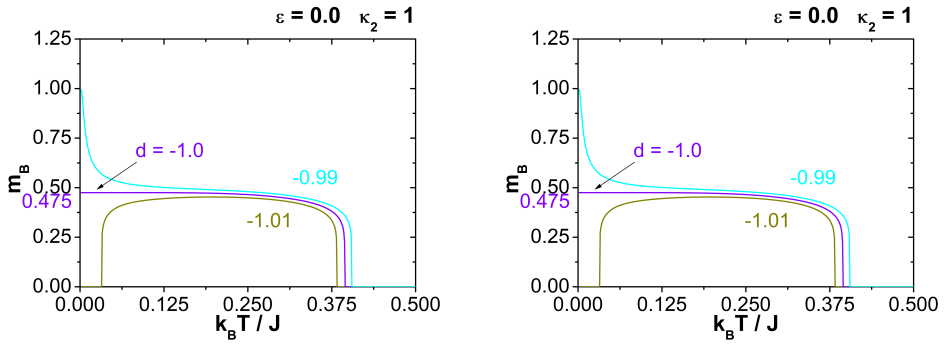

Fig. 8.7: The temperature dependence of sublattice magnetizations m_A and m_B for $\varepsilon = 0.0$, $\kappa_2 = 1$ and three representative values of d.

anisotropy values from a narrow region $d \in \langle -1.061, -1 \rangle$. These closed curves of the critical temperature reveal a special issue, when with the decreasing temperature the system firstly proceeds from a disordered phase to the ordered one (which is inside of the self-closed line) and then reaches again the disordered phase which extends down to zero temperature. The appearance of partially ordered phase with (m_A, m_B) = (0.475, 0.475) can be definitely confirmed from the study of thermal variations of magnetization down to zero temperature, by selecting the values of crystal field from the neighborhood of $d = -1.0$. In Figs. 8.6 and 8.7 there are depicted the thermal dependencies of sublattice magnetizations for $\varepsilon = 0.5$ and $\varepsilon = 0.0$, respectively, selecting three typical values of the crystal field a putting $\kappa_2 = 1$. The presented dependencies are in a perfect agreement with the ground-state analysis and they also clearly demonstrate the existence of partially ordered phase for $d = -1$, as well as, the reentrant behavior (see the curve for $d = -1.01$).

9 Conclusion and future perspective

In this work we have reviewed experimental and theoretical studies dealing with higher-order interactions. In particular, we have focused our attention on the detailed discussion of magnetic systems with higher-order spin interactions. In general, there are many kinds of multispin interactions that can be relevant for the description of many real magnetic compounds. In order to enlighten the impact of higher-order spin interactions in magnetic systems, we have in Sec. 2 extensively reviewed research works treating this subject both experimentally and theoretically. We have discussed many interesting physical phenomena, understanding of which requires to go beyond the standard physical picture based on the pair bilinear interactions only. As it follows from our discussion, the most important higher-order interactions in magnetic systems are the four-spin ones. The existence and impact of these interactions has been experimentally established in many real magnetic compounds and these observations have initiated the development of theoretical methods that are able to incorporate the energy terms with higher-order spin interactions and explain experimental data. Many novel results that are closely related to the four-spin interactions have been accumulated over decades and therefore, we have tried in Sec. 3 to classify these interactions in a logical manner. The particular attention has been payed to the explanation of three-site four spin interactions, which can be related to the magneto-elastic and magnetostriction phenomena. In fact, this type of interactions has a very special kind of symmetry with respect to the spin reversal procedure and therefore these interactions may produce some unexpected physical phenomena in magnetic systems.

Here it is necessary to emphasize, that the theoretical investigation of multispin interactions in magnetic systems is as a rule based on various Ising and Heisenberg models, which are able to incorporate higher-order spin interaction energy terms in a simple and consistent manner. Moreover, the theoretical studies based on Ising and Heisenberg models may provide even exact results for all relevant physical quantities. Taking into account this important feature and owing also to some exclusivity of the three-site four-spin interactions, we have in the second part of this work reviewed in detail recent theoretical results obtained for different exactly solvable mixed-spin Ising models with three-site four-spin interactions on various decorated lattices. It follows from our analysis that this kind of higher-order spin interactions initiates the appearance of several unconventional partially ordered magnetic phases, that may exhibit different non-zero values of the entropy at $T = 0.0$. Moreover, the careful analysis of the exactly solvable mixed-spin Ising model on the decorated triangular lattice with magneto-elastic coupling has revealed that the partially disorder phase may be found also in the standard decorated models with pair interactions and crystal field only.

Without any doubts, the research of higher-order interactions in general, and investigation of magnetic spin systems with multispin interactions in particular, represent a very important field of study which deserves in the future much more attention both from experimental and theoretical physicists. The future development of this research field will definitely help to understand observed experimental data in many magnetic compounds and from the viewpoint of basic physics it has a potential to discover new physical phenomena originating deeply from the new symmetries present in the systems with higher-order interactions.

Acknowledgments

Acknowledgement: This work was financially supported by the grant of Scientific Grant Agency of The Ministry of Education, Science, Research, and Sport of the Slovak Republic under contract No. VEGA: 1/0531/19 and by the grant of Slovak Research and Development Agency provided under contract No. APVV 16-0186.

References

[1] W. Selke, K. Binder, and W. Kinzel, Surf. Sci. 125, 74 (1983); R. C. Kittler and K. H. Bennemann, Solid State Commun. 32, 403 (1979).

[2] B.Held and C. Deutsch, Phys. Rev. A 24, 540 (1981).

[3] C. W. Wong and T. Sawada, Ann. Phys. N.Y. 72, 107 (1972).

[4] J. M. Delrieu and N. S. Sullivan, Phys. Rev. B 23, 3197 (1981).

[5] R. J. Baxter, Ann. Phys. (N.Y.) 72, 107 (1972).

[6] R. J. Baxter and F. Y. Wu, Phys. Rev. Lett. 21, 1294 (1973).

[7] M. Suzuki, Phys. Rev. Lett. 28, 507 (1972).

[8] F. Y. Wu and H. E. Stanley, Phys. Rev. 8 26, 6326 (1982).

[9] C. Kittel, Phys. Rev. 120, 335, (1960).

[10] E. A. Harris and J. Owen, Phys. Rev. Lett. 11, 9, (1963).

[11] D.S. Rodbell. I.S., Jacobs, J. Owen and E.A. Harris, Phys. Rev. Lett. 11, 10 (1963).

[12] Köbler U, Mueller R M, Schnelle W and Fischer K, J. Magn. Magn. Mater. 188, 333 (1998).

[13] Mueller R M, Köbler U and Fischer K, Eur. Phys. J. B 8, 207 (1999).

[14] Köbler U, Mueller R, Smardz L, Maier D, Fischer K, Olefs B and Zinn W, Z. Phys. B 100, 497 (1996).

[15] Müller-Hartmann E, Köbler U and Smardz L, J. Magn. Magn. Mater. 173, 133 (1997).

[16] Köbler U, Hoser A, Graf H A, Fernandez-Diaz M-T, Fischer K and Br¸ckel Th, Eur. Phys. J. B 8, 217 (1999).

[17] U. Köbler, K. Fischer, J. Phys.: Condens. Matter 13, 123 (2001).

[18] U. Köbler, R.M. Mueller, P.J. Brown, R.R. Arons, K. Fischer, J. Phys.: Condens. Matter 13, 6835 (2001).

[19] U. Köbler, A. Hoser, D. Hupfeld, Physica B 328, 276 (2003).

[20] U. Köbler et al., Physica B 355, 90–99 (2005).

[21] U. Köbler, A. Hoser, R. M. Mueller, K. Fischer, J. Magn. Magn . Mat. 315, 1, 12-25 (2007).

[22] M. Roger, H. M. Delrieu, J. H. Hetherington, Rev. Mod. Phys. 55, 1 (1983).

[23] M. Date, T. Sakakibara, K. Sugiyama, H. Suematsu, High Field Magnetism (1983).

[24] T. Iwashita, N. Uryu, Phys. Lett. A 155, 4 (1991).

[25] T. Iwashita, N. Uryu, J . Phys. Soc. Japan 36, 48-54 (1974).

[26] T. Iwashita, N. Uryu, J. Phys. C: Solid State Phys. 17, 855-868 (1984).

[27] D. W. Wood, H. P. Griffiths, J. Math. Phys. 14, 1715 (1973).

[28] H. P. Griffiths, D. W. Wood, J. Phys. C 6, 2533 (1973).

[29] D. W. Wood, H. P. Griffiths, J. Phys. C 7, 1417 (1974).

[30] D. W. Wood, H. P. Griffiths, J. Phys. C 7, L54 (1974).

[31] H. P. Griffiths, D. W. Wood, J. Phys. C 7, 4021 (1974).

[32] J. Ho-Ting-Hun, J. Oitmaa, J. Phys. A 9, 2125 (1976).

[33] R. V. Ditzian, Phys. Lett. 42A, 67 (1972).

[34] O. Mitran, J. Phys. C 12, 557 (1979); 12, 4871 (1979).

[35] O. Mitran, Ph.D. thesis, Concordia University, Montreal, (1979).

[36] B. Frank, J. Phys. C 12, L595 (1979).

[37] M. Gitterman, M. Mikulinsky, J. Phys. C 10, 4073 (1977).

[38] S. Lacková, M. Jaščur, J. Magn. Magn. Mat. 217 (2000) 216.

[39] V. M. Matveev, E. L. Nagaev, Fiz. Tverd. Tela (Leningrad) 14, 492 (1972), Sov. Phys.-Solid State 14, 408 (1972).

[40] O. G. Mouritsen, S. J. Knak Jensen, B. Frank, Phys. Rev. B23, 976 (1981).

[41] O. G. Mouritsen, S. J. Knak Jensen, B. Frank, Phys. Rev. B 24, 347 (1981).

[42] R. Li, T. Numazawa, T. Hashimoto, A. Tomokiyo, T. Goto, S. Todo, Advances in Cryogenic Engineering Materials 32, 287-294 (1986).

[43] W. P. Wolf, Braz. J. Phys. 30, 4, 794-810 (2000).

[44] R. J. Baxter, F. Y. Wu, Phys. Rev. Lett. 31, 1294 (1973).

[45] J. Oitmaa, R. W. Gibberd, J. Phys. C 6, 2077 (1973).

[46] J. Oitmaa, ibid. 7, 389 (1974).

[47] F. Y. Wu, J. Phys. C 9, L23 (1977).

[48] K. Jungling, J. Phys. C 9, L139 (1976).

[49] D. Imbro, P. C. Hemmer, Phys. Lett. 57A, 297 (1976).

[50] S. Froyen, Aa. S. Suds, P. C. Hemmer, Physica 85A, 399 (1976).

[51] M. Yamashita, H. Nakano, K. Yamada, Prog. Theor. Phys. 62, 1225 (1979).

[52] I. Syozi, Prog, Theor. Phys. 34, 189 (1965); I. Syozi and S. Miyazima, Prog. Theor, Phys. 36, 1083 (1966).

[53] M. Matsuura, Y. Ajiro, T. Haseda, J. Phys. Soc. Japan 26, 665 (1969).

[54] K. Takeda, M. Matsuura, T. Haseda, J. Phys. Soc. Japan .28, 29 (1970).

[55] A. A. Stepanov, P. Wyder, T. Chattopadhyay, P. J. Brown, G. Fillion, I. M. Vitebsky, A. Deville, B. Gaillard, S. N. Barilo, D. I. Zhigunov, Phys. Rev. B 48, 12979 (1993).

[56] T. Sakakibara, K. Sugiyama, M. Date, H. Suematsu, Synthetic Metals, 6, 165 - 172 (1983).

[57] D. D. Osheroff, M. H. Cross and D. S. Fisher, Phys. Rev. Lett. 44, 792 (1980).

[58] M. Roger, J. Delrieu, J. Hetherington, Journal de Physique Colloques, 41 (C7), C7-241-C7-248, (1980).

[59] J. Hara and H. Fukuyama: Technical Report of ISSP, Ser A, No.1129 (1981).

[60] J. M. Hastings and L. M. Corliss, IBM J. Res. Dev. 14, 227-228 (1970).

[61] T. Miyadai, K. Takizawa, H. Nagata, H. Ito, S. Miyahara, K. Hirakawa, J. Phys. Soc. Jpn. 38, 115-121 (1975).

[62] H. Nagata, H. Ito, T. Miyadai, J. Phys. Soc. Jpn. 41, 2133 (1976).

[63] K. Yosida, S. Inagaki, J. Phys. Soc. Jpn. 50, 3268-3277 (1981).

[64] J. Rouchy, P. Morin, J. Magn. Magn. Mater. 23, S 59-68 (1981).

[65] J Rossat-Mignod et al, J. Phys. C: Solid State Phys. 13, 6381 (1980).

[66] T. Takeda, K. Konishi, H. Deguchi, N. Iwata, T. Shigeoka, J. Magn. Magn. Mater. 9013, 104-107 (1992).

[67] Y Muraoka et al, J. Phys. A: Math. Gen. 27, 2675 (1994).

[68] J. C. Slonczewski, J. Appl. Phys. 73, 5957 (1993).

[69] A. Fuß, S. Demokritov, P. Grunberg, W. Zinn, J. Mag. and Mag. Mat. 103, 3, L221-L227 (1992).

[70] M. I. Belinsky, Chemical Physics, 223, 195 - 210 (1997).

[71] H. Lin, L. Rebelsky, M. F. Collins, J. D. Garrett, W. J. L. Buyers, Phys. Rev. B 43, 13232(1991).

[72] A. Mailhot, M. L. Plumer, A. CaillÈ, and P. Azaria, Phys. Rev. B 45, 10399 (1992).

[73] S. W. Zochowski, S.A. Creeger and M.F. Collins, J. Magn. Magn. Mat. 140-144 (1995) 1399 - 1400.

[74] T. Shiroka et al., Carbon 63, 294–302 (2013).

[75] G. Lamura, T. Shiroka, N. Emery, H. Rida, S. Cahen, J-F. Mareche, et al., Carbon 50(4), 3995–4001 (2012).

[76] F. Y. Wu, Phys. Rev. B 4, 7 (1971).

[77] L. P. Kadanoff, F. J. Wegner, Phys. Rev. B4, 3989-93 (1971).

[78] Ann. Phys., NY 70, 193-228 (1972).

[79] R. J. Baxter, F. Y. Wu, Aust. J. Phys. 27, 357-67 (1974).

[80] R.G. Munro, M.D. Girardeau, J. Magn. Magn. Mat. 2 (1976).

[81] G. H. Jonker, J. H. Van Santen, Physica 16, 337 (1950).

[82] C. Zener, Phys. Rev. 81, 440 (1951).

[83] T. Iwashita and N. Uryu, J. Phys. C: Solid State Phys. 12, (1979).

[84] T. Oguchi, Prog. Theor. Phys. 13, 148 (1955).

[85] P. Kulish , E. Sklyanin, Integrable Quantum Field Theories, edited by J. Hietarinta and C. Montonen, Lecture Notes in Physics Vol. 151 (Springer-Verlag, Berlin, 1982), p. 61; P. Kulish, N. Yu. Reshetikhin, E. Sklyanin, Lett. Math. Phys. 5, 393 (1981); L. Takhtajan, Phys. Lett. 87A, 479 (1982); J. Babudjian, Phys. Lett. 90A, 479 (1982) and Nucl. Phys. B215, 317 (1983).

[86] I Affleck, et al., Phys.Rev.Lett. 59, 799 (1987).

[87] W. Buyers, R. Morra, R. Armstrong, M. Hogan, P. Gerlack, K. Hirakawa, Phys. Rev. Lett. 56, 371 (1986).

[88] F. Mila, Fu-Chun Zhang, Eur. Phys. J. B 16, 7-10 (2000).

[89] O. G. Mouritsen, B. Frank, D. Mukamel, Phys. Rev. B 27, 3018 (1983).

[90] P. J. Jensen, K. A. Penson, K. H. Bennemann, Phys. Rev. A 40, 1681, (1989).

[91] M. Grynberg, H. Ceva, Phys. Rev. B 40, 7265 (1989).

[92] J. M. Debierre, L. Turban, J. Phys. A 16, 3571 (1983).

[93] A. N. Berker, Phys. Rev. B 12, 2752-8 (1975).

[94] K. A. Penson, Phys. Rev. B 29, 2044 (1984).

[95] M. Kolb, K. A. Penson, Phys. Rev. B 31, 3147 (1985); J. Appl. Phys. 57, 3325 (1985).

[96] M. D. Grynberg, H. Ceva, Phys. Rev. B 36, 7091 (1987).

[97] H. Ceva and J. A. Riera, Phys. Rev. B 38, 4705 (1988).

[98] H. L. Scott, Phys. Rev. A 37, 263 (1988).

[99] L. Hernandez, H. Ceva, Phys. Rev. B 43, 698 (1991).

[100] C. Buzano, M. Pretti, Phys. Rev. B 56, 636, (1997).

[101] A. W. Sandvik, Phys. Rev. Lett. 98, 227202 (2007).

[102] J. L. Lebowitz, D. Ruelle, Commun. Math. Phys. 304, 711 (2011).

[103] N. Benayad, M.Ghliyem, Physica B 407 (2012).

[104] M. Jaščur, S. Lacková, J. Phys.: Condens. Matter 12, L1-L7 (2000).

[105] S. Lacková, T. Horiguchi, M. Jaščur, Physica A 326, 189-202 (2003).

[106] S. Lacková, M. Jaščur, Physical Review E 64, 036126-1-6 (2001).

[107] T. Iwashita, N. Uryu, J. Phys. C: Solid State Phys. 21, 4783 (1988).

[108] Y. Muraoka et al, J. Phys. A: Math. Gen. 26, 1811 (1993).

[109] E. Müller-Hartmann, U. Köbler, L .Smardz, J. Magn. Magn. Mat. 173, 133-140 (1997).

[110] Y. Muraoka, Phys. Rev. B 64, 134416 (2001).

[111] F. Honda, *Doctor thesis*, Kumamoto University, (2000).

[112] G. Quirion, F.S. Razavi, M.L. Plumer, and J.D. Garrett, Phys. Rev. B 57, 5220 (1998).

[113] J. P. Joule, The London, Edinburgh and Dublin philosophical magazine and journal of science (Taylor & Francis) 30, Third Series: 76–87, 225–241, (1847).

[114] L. Néel, Bull. soc. franc. mineral. crist. 77, 257 (1954).

[115] E. A. Harris, J. Phys. C: Solid State Phys., Vol. 5, (1972).

[116] J. Strečka and M. Jaščur, Acta Physica Slovaca 65, 235 (2015).

[117] I. Syozi, Prog. Theor Phys. 6, 306 (1951).

[118] L. Onsager, Phys. Rev. 65, 117 (1944).

[119] V. Štubňa, Exactly solvable lattice models with multispin interaction, *Thesis for dissertation exam*, UPJŠ, Institute of Physics, Košice, (2015).

[120] M. Jaščur, V. Štubňa, K. Szalowski, T. Balcerzak, Acta Physica Polonica 126, 48 (2014).

[121] M. Jaščur, V. Štubňa, T. Balcerzak, K. Szalowski, J. Magn. Magn. Mater. 417, 92 (2016).

[122] V. Štubňa, M. Jaščur, J. Magn. Magn. Mater. 442, 364 (2017).

[123] H. B. Callen, Phys. Lett. 4, 161 (1963).

[124] M. Suzuki, Phys. Lett. 19, 267 (1965).

[125] R. Honmura, T. Kaneyoshi, J. Phys. C 12 (1979).

[126] T. Kaneyoshi, J.W. Tucker, M. Jaščur, Physica A 186, 495-512 (1992).

[127] C. N. Yang, Phys. Rev. 85, 808 (1952).

[128] M. Jaščur, Physica A 252 (1998) 217.

[129] R. M. F. Houtappel, Physica 16, 425 (1950).

[130] H. N. V. Temperley, Proc. R. Soc. London A 203, 202 (1950).

[131] G. H. Wannier, Phys. Rev. 79, 357 (1950); erratum: Phys. Rev. B 7, 5017 (1973).

[132] C. Domb, Adv. Phys. 9, 149 (1960).

[133] R. B. Potts, Phys. Rev. 88, 352 (1952).

[134] I.G. Enting, J. Phys. A: Math. Nucl. Gen. 6, 170 (1973).

[135] J. Strečka, O. Rojas, S.M. de Souza, Physics Letters A 376, 3, 197-202 (2012).

Professor Michal Jaščur received his PhD degree in condensed matter physics in 1995 from P. J. Šafárik University in Košice under supervision of Prof. Andrej Bobák. In 2000 he defended the habilitation in physics and since then until 2014 he served at P. J. Šafárik University in Košice as an associate professor. Now he holds the position of full professor in physics at the same institution. In the past he spent two years as a researcher under supervision of Prof. Takahito Kaneyoshi at Nagoya University. He also was JSPS fellow and for many years he develops a research collaboration with Prof. Tadeusz Balcerzak and Dr. Karol Szalowski from the University of Lodzi in Poland. His primary research interests are in the condensed matter theory including an investigation of magnetic, thermal, electron and elastic properties of various physical systems.

RNDr. Ing. Viliam Štubňa, PhD. received his PhD degree in the field of general and mathematical physics in 2019 from P. J. Šafárik University in Košice under supervision of Prof. Michal Jaščur. Within his study he spent three months as a researcher at JINR Dubna working on development of various mathematical methods using parallel programming in CUDA environment. His research interests cover the statistical physics and its applications to magnetic systems, mainly those with the higher-order interactions.